Utrecht University

Bicontinuous Janus Materials

Steffen Lootsma

Master Thesis Nanomaterials Science

Supervisors:

dr. M. F. Haase

dr. M.A. Khan

Graduate School of Natural Sciences

Debeye Institute for Nanomaterials Science

Physical and Colloidal chemistry Group

Van't Hoff laboratorium

Abstract

Hydrogen fuel cells can contribute to the transition to a more sustainable global society. Hydrogen and oxygen are used for the conversion of chemical energy to electrical energy, with water as a waste product. There is a limiting factor however to the power density output of these cells. At high humidity water condenses inside the pores of the gas diffusion layer (GDL), reducing the oxygen uptake of the cell. GDLs with patterned wettability can mitigate this problem. We propose the use of a porous Janus material, with asymmetric surface properties as GDL to provide separate pathways for the diffusion of oxygen and the removal of water from the cell. Bicontinuous interfacially jammed emulsion gels (bijels) are used as precursor for such a material. Bijels have a unique morphology with interpenetrating oil and water channels separated by a layer of nanoparticles. By selective hydrophobization of the nanoparticle scaffold inside a bijel, a Janus material can be obtained. The surface modification is done using alkyl silanes, more specific octadecyl trichlorosilane. Different reaction times and concentrations are studied to obtain the optimal effect. With Scanning Electron Microscopy (SEM) and Scanning Laser Confocal Microscopy the modified bijels are characterized, where Reconstitution experiments are executed to monitor the wetting behavior of hydrophobic and hydrophilic liquids inside the pores of the treated bijel scaffold.

Contents

1. Introduction

As the global community moves towards greater sustainability and environmental responsibility, it is crucial to explore diverse pathways for the generation of zero-emission energy. One promising approach involves the use of hydrogen fuel cells, which convert chemical energy from hydrogen gas into electrical energy while producing only water as a waste product[1]. A hydrogen fuel cell comprises three major components: The anode, where hydrogen gas undergoes oxidation and electrons are removed from the species. The cathode, where oxygen O_2 is reduced to O^- by the addition of electrons, and react with protons from the anode to form water. Lastly, an electrolyte material separates the anode and cathode, acting as a proton membrane (PEM) that exclusively permits the transport of H^+ ions while electron transport is inhibited[2]. Another crucial part in these fuel cells is the gas diffusion layer (GDL), which not only has the function to distribute reactant gases to the electrode surface but is also responsible for the water management[3]. Typically, GDLs are constructed using carbon fiber paper or carbon fiber cloth[1]. A key limiting factor in the production of energy in hydrogen fuel cells is a phenomenon called 'flooding'. This occurs at high levels of humidity, where the gas flow field channels of the GDL can become obstructed due to the presence of water[4]. Recent studies have revealed that diffusion layers with patterned wettability, featuring hydrophilic and hydrophobic pathways, can significantly reduce the impact of flooding on cell performance[5,6]. Janus materials inherently possess these properties[7].

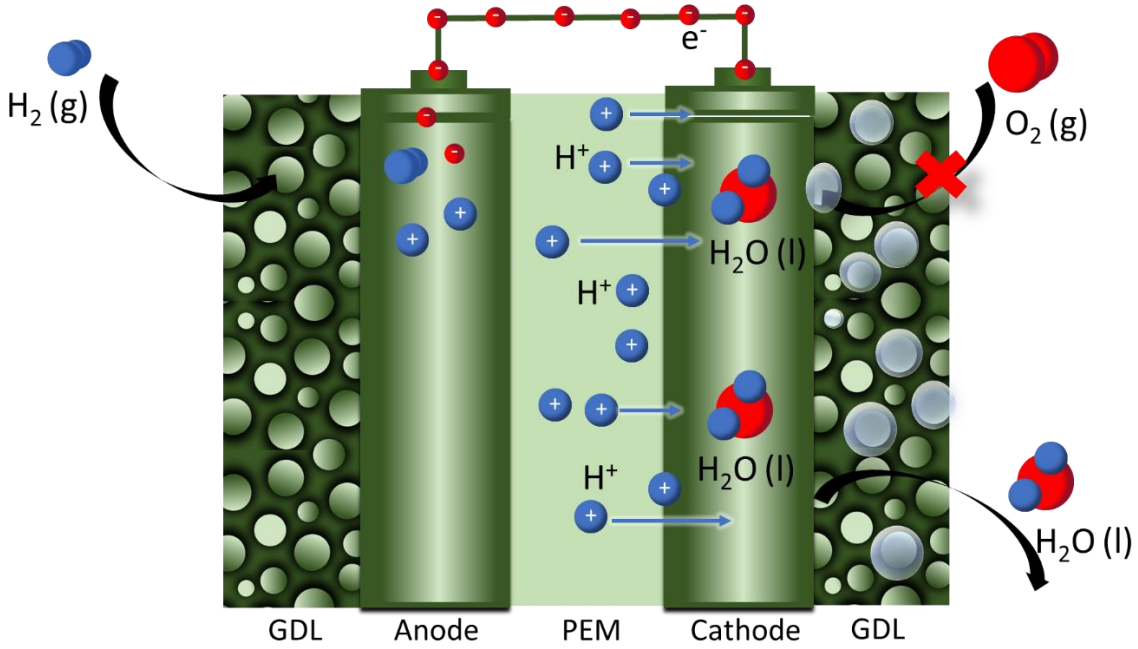

Figure 1. *Schematic representation of the flooding of a Proton Exchange Membrane Hydrogen Fuel cell (PEMFC). Hydrogen gas is guided to the Anode through a gas diffusion layer (GDL), here H_2 is converted to protons that are guided through the membrane (PEM) and electrons through the circuit. At the Cathode oxygen, protons and electrons form water, that is removed through the GDL, blocking the O_2 uptake.*

Janus was the Roman gatekeeper god of the past and the future. Janus was considered one of the Numina, which can be translated as the powers of the will. Janus was the god of good beginnings that ensured good endings. The first month of the year January is named after him, and in ancient Rome there was a temple dedicated to Janus. The temple ran from east to west, where the sun rises and sets. This temple contained a statue of Janus and was located between two doors. The statue had two faces, a young one and an old one, symbolizing his role as god of transitions[8].

Analogous to the two faced head, the key characteristic of Janus materials are the asymmetric surface properties such as wettability, charge, pore size and conductivity[9]. The interest in Janus materials was primarily focused on the nano- and micrometer scale. The first experimentally synthesized Janus material was Janus beads or J-beads, which consist of glass spheres where half of the sphere is uniformly covered with aliphatic chains to create an amphiphilic solid with a hydrophilic and hydrophobic side[10]. Other types of Janus materials with different morphologies such as Janus -rods, -disks, and -sheets, have also been investigated[7]. Recently, the interest in Janus materials has expanded to the macroscopic scale, particularly in the case of porous Janus materials. Janus characteristic of porous materials allows their usage for a wide range of applications, including separation, filtration and catalysis[12-13].

Porous Janus materials can be categorized into two types of working mode: synergistic and independent. Synergistic porous Janus materials exhibit unique diode performance and can facilitate directional liquid transport, to create for instance water-oil diodes. Independent porous Janus materials are multifunctional and integrated, where the asymmetric properties work independently without interfering with each other[9]. In this research we are interested in using Bicontinuous interfacially jammed emulsion gels (bijels) as template for independent porous Janus materials.

Bijels are a unique type of material defined by two interpenetrating liquid phases, an oil and a water phase, separated by a stabilizing interfacial layer. The structure arises from the spinodal decomposition of a precursor mixture containing two immiscible liquids, which creates continuous networks of interconnected channels that are stabilized by nanoparticles at the liquid-liquid interface[14,15]. The distinctive bijel morphology allows for in situ surface modification by means of a single phase to impart hydrophobicity to only one side of the nanoparticle network, while the other side remains hydrophilic. This can be done by letting alkyl-silanes diffuse inside the oil channels of a bijel, which can subsequently be hydrolyzed, condensed and polymerized onto the particle surface at the oil-water interface. A similar procedure already showed to be successful for the reinforcement of the particle scaffold by crosslinking the system with Tetraethyl orthosilicate (TEOS)[16]. We hypothesize that after the removal of the liquids from the bijel, a selectively hydrophobized nanoparticle scaffold

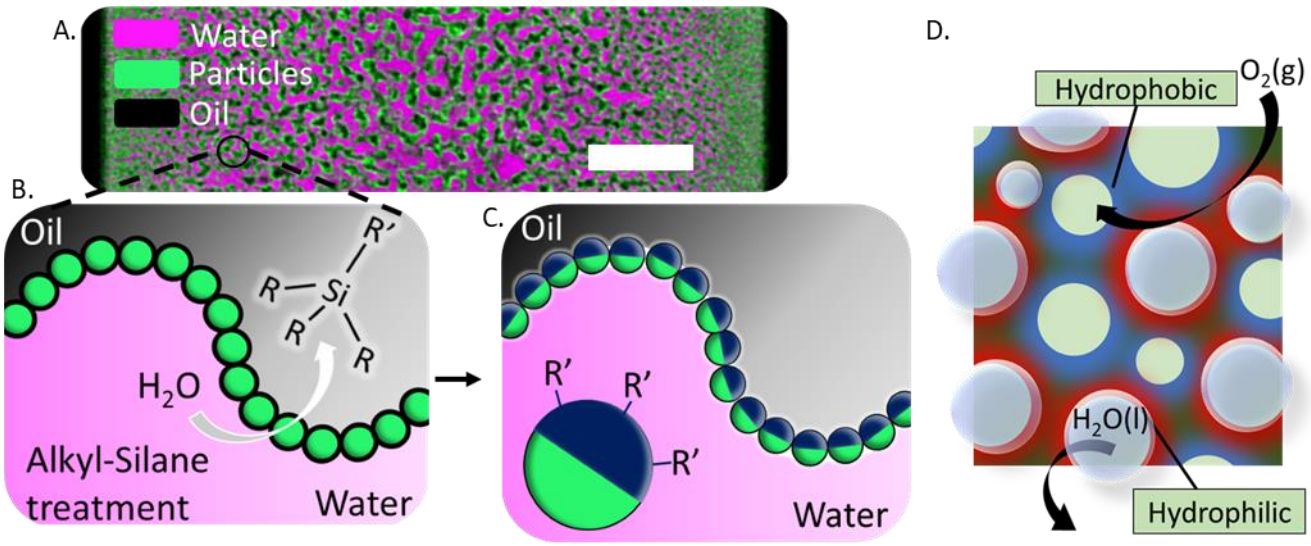

***Figure 2**. Selective hydrophobization of bijels **A.** Confocal micrograph of a bijel **B.** Alkyl silane treatment of a bijel **C.** Janus porous network inside bijel. **D.** Janus porous material with asymmetric surface properties.*

is obtained. This creates a material that contains a hydrophobic pore network intertwined with the untreated hydrophilic pores.

This type of material perfectly suites the purpose of the GDL. The hydrophobic pore network guides diffusion of oxygen gas towards the cathode. This process is not disturbed by the presence of water as the independent hydrophilic pore network facilitates the removal of water from the cell.

The aim of this project will be to selectively hydrophobize the nanoparticle scaffold of a bijels, thereby creating independent janus materials. We hypothesize that by insitu treatment of bijel fibers with octadecyltrichlorosilane (OTS) this selective hydrophobization can be realized. Our focus will be on studying the factors affecting the stability of bijels and improve the selective hydrophobization by varying the main parameters such as OTS concentration and time of treatment. The methods that will be used to test this hypothesis include Scanning Electron Microscopy (SEM) to investigate the change of morphology of the nanoparticle scaffold, and Scanning Laser Confocal Microscopy (SLCM) to monitor the wetting behaviour of hydrophilic and hydrophobic liquids inside the treated bijel scaffold using solvatochromic dyes to probe the local hydrophobicity inside the bijel pores.

2. Theoretical section

2.1 Hydrophobic and Hydrophilic surfaces

The desired Janus porous material that can act as a gas diffusion layer, must contain hydrophilic pores that attract water and transfer it out of the cell and hydrophobic pores that repel water and allow for gases to enter the cell. In general, the ability of a liquid to stay in contact with a solid surface is called wetting. The degree of wetting is determined by the cohesive intramolecular forces of the liquid, and the adhesive intermolecular forces between the surface and the liquid. [17]

For liquid water the attraction between water molecules is mainly governed by hydrogen bonds that have a strongly directional character. In bulk water, Each water molecule forms an average of 3 hydrogen bonds with neighboring water molecules, resulting in an equal strength of the forces in all directions.[18] At the water-air interface however the intramolecular forces are no longer balanced because the surface molecules are not able to form the same amount of hydrogen bonds. Therefore the surfaces molecules are more attracted to each other, and a net pull into the bulk phase of the liquid is experienced. This phenomenon is called surface tension: γ [N/m]. Surface tension is responsible for the formation of water droplets and bubbles, because it drives towards the minimization of the surface area of water.[19]

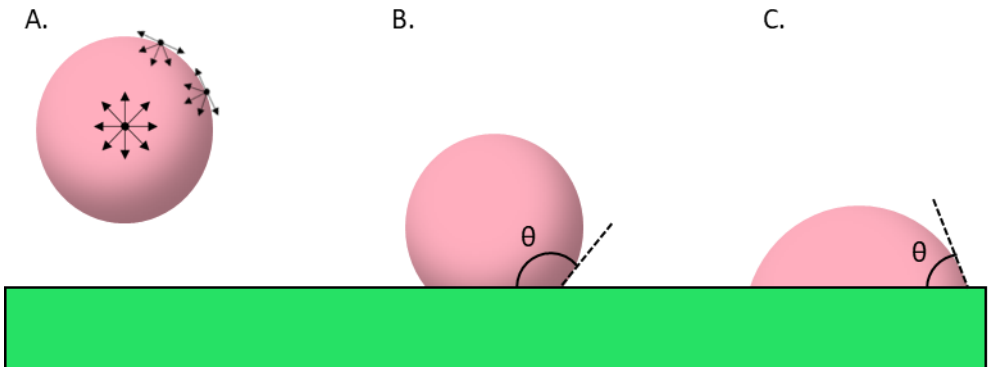

Figure 3. *Water droplets in different environments.* ***A.*** *water droplet in air, the arrows representing amount of hydrogen bonds that can be formed.* ***B.*** *water droplet on a hydrophobic surface with ϑ > 90°.* ***C.*** *water droplet on a hydrophilic surface with θ > 90°.*

When water comes into contact with a solid surface, the wettability of the surface can be described by the three phase contact angle (θ) between water, air and the solid surface.[20] The contact angle is conventionally measured from the water phase. When the surface is eager to form hydrogen bonds

with water, the interaction of water with the surface is favored above the interaction with air. This causes the water to spread over the surface corresponding to a contact angle < 90°, the surface is said to be hydrophilic.[21] The opposite is true for a surface that doesn't like to form hydrogen bonds. These surfaces have contact angels > 90° and are hydrophobic. The relation between the interfacial forces and the contact angle are described by Youngs equation.[22] Where γ is the interfacial tension between the solid-gas (SG), solid-liquid (SL) and Liquid-Gas (LG) phase.

$$\gamma_{SG} - \gamma_{SL} - \gamma_{LG} * \cos(\theta) = 0 \quad (1)$$

The interfacial gibbs free energy can be calculated using equation (2) [23], where dG is the the change in gibbs free energy, γ the interfacial tension and dA the change in surface area.

$$dG = \gamma dA \quad (2)$$

2.2 Particle stabilized emulsions

For this research we want to modify the interior surface of bijels, to obtain a nanoparticle scaffold with hydrophobic and hydrophilic pores. As bijels are a special type of particle stabilized emulsion, a quick introduction to the subject is given starting with the different types of emulsions. Emulsions can be classified into two primary categories: water in oil (W/O) emulsions, where water droplets are dispersed in a continuous oil phase, and oil in water (O/W) emulsions, where oil droplets are dispersed in a continuous water phase. Common examples for W/O emulsions are creamy substances such as cosmetic skin products, while typical examples of O/W emulsions are edibles such as milk or mayonnaise. [24,25] The droplet size is typically on the colloidal scale (nm-µm), but not strictly bound to this size range, and emulsion droplets can also be hundreds of micrometers in size.[26] Emulsifiers play a crucial role in the stabilization of emulsions, by reducing the interfacial tension between the liquids and preventing flocculation, Ostwald ripening and coalescence. Emulsifiers possess amphiphilic properties and can be proteins like casein in milk or surfactants with polar head groups and apolar tail groups.[27] Nanoparticles can also serve as stabilizers for emulsions leading to the formation of Pickering emulsions.[28]

When nanoparticles are used to stabilize an emulsion, the wettability of the particles determines the type of emulsion that can be stabilized. When the particles are predominantly hydrophobic, the particles prefer to be in the oil phase over the water phase. These particles with a contact angle of >90°, favor the stabilization of W/O emulsions. The opposite is true for predominantly hydrophilic particles with a contact angle of <90°, favoring the stabilization of O/W emulsions.[29]

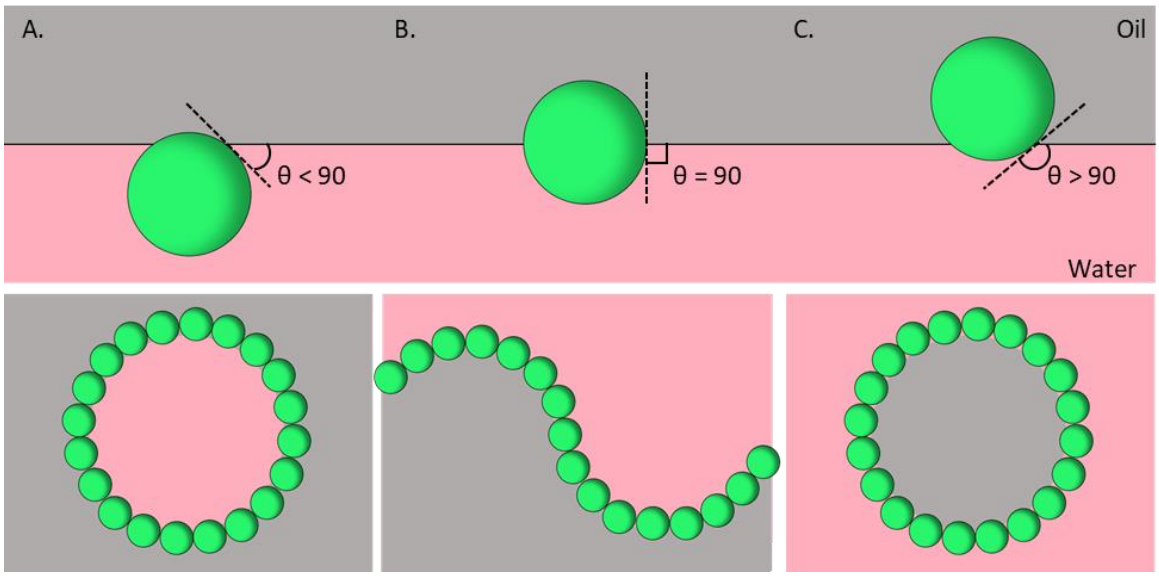

Figure 4**. Schematic representation of particles with different wettability's.* ***A. *Hydrophilic particles stabilizing W/O emulsions* ***B.*** *Neutral wetting particles without preferred stabilization, allowing Bicontinuous domains.* ***C.*** *Hydrophobic particles stabilizing O/W emulsions.*

The nanoparticles reduce the unfavorable contact between water and oil. The attachment energy of the particles depends on the wettability and can be calculated using equation (1) and (2).[30,31] We consider a particle that is completely submerged in water (5.A), and a particle at the interface between oil and water (5.B). The Gibbs free energy can be calculated for both situations G_1 for a completely submerged particle and G_2 for a particle at the interface. The difference in energy gives the attachment energy for a particle at the interface. Here the surface area for the oil water interface is given by $A_{ow}^{(1)}$and $A_{ow}^{(2)}$, for a particle in water and at the interface respectively. The surface area of the particle is given by A_p, the particle facing the oil by A_{po} and the particle facing water by A_{pw}. The interfacial tension is given by γ_{ow}, $\gamma_{pw,}$ γ_{po} for the oil-water, particle-water and particle-oil interface respectively. The attachment energy is derived by the following equations:

$$\Delta A_{ow} = A_{ow}^{(1)} - A_{ow}^{(2)}, \text{ and } A_p = A_{pw}^{(2)} + A_{po}^{(2)}. \quad (2)$$

$$G_1 = \gamma_{ow}A_{ow}^{(1)} + \gamma_{pw}A_p \quad (3)$$

$$G_2 = \gamma_{ow}A_{ow}^{(2)} + \gamma_{pw}A_{pw}^{(2)} + \gamma_{po}A_{po}^{(2)} \quad (4)$$

$$\Delta G = G_2 - G_1 = \gamma_{ow}\Delta A_{ow} + (\gamma_{pw}A_{pw}^{(2)} + \gamma_{po}A_{po}^{(2)}) - (\gamma_{pw}A_{pw}^{(2)} - \gamma_{pw}A_{po}^{(2)}) \quad (5)$$

$$\Delta G = \gamma_{ow}\Delta A_{ow} + (\gamma_{po} - \gamma_{pw})A_{po}^{(2)} \quad (6)$$

Using equation (1) , $\gamma_{po} - \gamma_{pw}$ can be written as $\gamma_{ow}\cos\theta$. This gives the following equation:

$$\Delta G = \gamma_{ow}\Delta A_{ow} + \gamma_{ow}\cos\theta\, A_{po}^{(2)} \quad (7)$$

$$\Delta G = \gamma_{ow}(\Delta A_{ow} + \cos\theta A_{po}^{(2)}) \quad (8)$$

Taken into account that the change in ow interface is equal to the surface of the intersection of the particle: $A_{ow}^{1} - A_{ow}^{2} = -\pi r^2 \sin^2\theta = -\pi r^2(1-\cos^2\theta)$, and A_{po} is equal to a spherical cap: $\cos\theta A_{po}^{2} = \cos\theta(2\pi r^2(1-\cos\theta))$ the following equation is obtained:

$$\Delta G = \gamma_{ow}[-\pi r^2(1-\cos^2\theta) + \cos\theta(2\pi r^2(1-\cos\theta))] \quad (9)$$

Where $[-\pi r^2(1-\cos^2\theta) + \cos\theta(2\pi r^2(1-\cos\theta))]$ can be rewritten to $-\pi r^2(1-2\cos\theta+\cos^2\theta) = -\pi r^2(1-\cos\theta)^2$. The Final expression for the attachment energy of spherical particles at the oil water interface yields:

$$\Delta G = -\pi r^2 \gamma_{ow}(1-\cos\theta)^2 \quad (10)$$

From this we can derive that particles with neutrally wetting surface properties (θ = 90°) result to a maximal attachment energy to the interface. Additionally there is no preference for stabilization of oil droplets in a continuous water phase or water droplets in a continuous oil phase for these particles, leading to bicontinuous liquid domains that can be stabilized with such particles. (figure 4.B)[32]

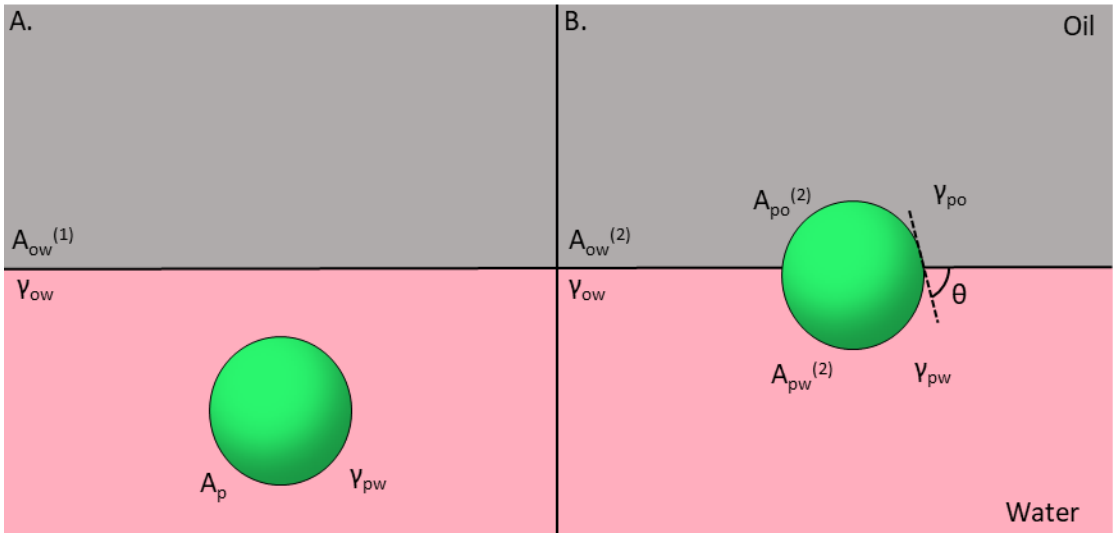

Figure 5. *Schematic representation of the attachment energy of a particle to the oil/water interface.* ***A.*** *Particle completely submerged in water. Where A_{ow}, γ_{ow} give the interfacial area and tension of the oil/water interface. A_p and γ_{pw} represent the interfacial area and tension of the particle in water.* ***B.*** *Particle at the o/w interface, with $A_{ow}^{(2)}$ the reduced interfacial area and A_{pw} and A_{po} representing the interfacial area of the oil and water phasing site of the particle respectively.*

2.3 Bicontinuous interfacially jammed emulsion gels

The Bicontinuous interfacially jammed emulsion gel or bijel is a material that was first speculated about in 2005, when computational studies were done regarding a material where a binary liquid was de-mixed via spinodal decomposition and the bicontinuous interface was stabilized and arrested by nanoparticles wetting both liquids equally.[33] This yields a unique type of soft material with an interwoven channel network of oil and water separated by a percolating layer of nanoparticles (6.A). In 2007 this was first experimentally realized by thermally quenching a liquid system containing 2,6-lutidine and water with neutral wetting silica colloidal particles (R_H = 290nm).[34] Lutidine and water mix at room temperature, but when the temperature is increased phase separation occurs. The mixture was quenched into critical conditions where phase separation occurs by spinodal decomposition. During phase separation an interface between the liquids is created, the nanoparticles present in the mixture are attracted to this interface to reduce the interfacial area between the liquids. As the interfacial area between the liquids decreases the particles get jammed at the interface, therefore the spinodal structure is arrested.

The thermal quenching process is subject to constraints imposed by a liquid system with low interfacial tension (γ_{ow}). As a result large particles are needed to ensure strong enough interfacial attachment for the stabilization of spinodal structures. These larger particles impose a limit to the bijel domain size to the micron scale (>5 µm). (6.B)

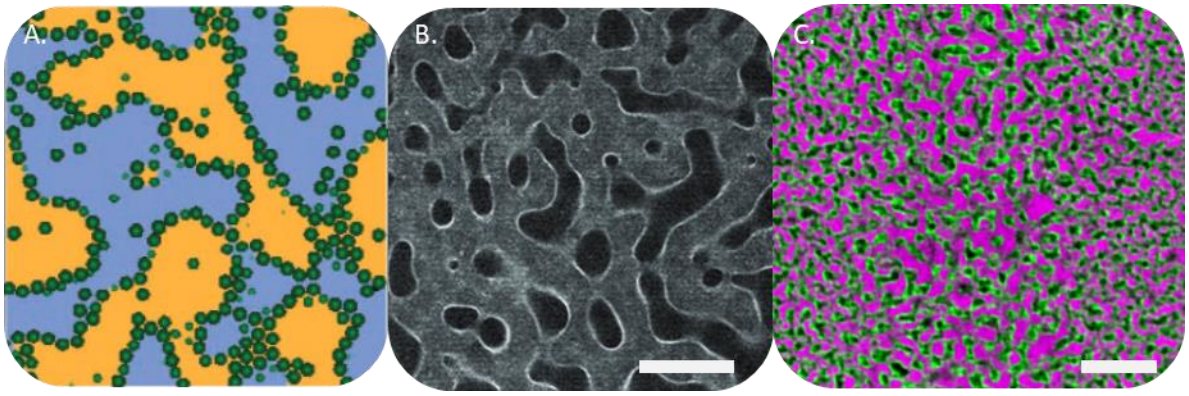

Figure 6**. Evolution of the Bicontinuous interfacially jammed emulsion geld.* ***A. *computational simulations[33]* ***B.*** *Thermal quenched bijel[34]* ***C.*** *STrIPS bijel[35,36]. The scalebars indicate 10µm*

In 2017 a novel synthesis pathway for bijels was introduced by Haase e.a.[35] Instead of increasing the temperature of a binodal mixture for phase separation, solvent transfer of a ternary mixture was used to realize spinodal decomposition of two immiscible liquids. Liquids with higher interfacial tension can be used, that can trap smaller particles and allow for the formation of bijels with sub-micron domains (300-500nm) throughout the entire structure (6.C).[36] A ternary precursor mixture is prepared by solving oil and water in alcohol and adding neutral wetting silica nanoparticles (ludox TMA) by addition of surfactants. Silica nanoparticles have hydroxyl surface groups that are deprotonated at sufficiently high pH resulting in a negative surface charge. With the adsorption of oppositely charged surfactants to the particles the wettability can be easily modified.

De-mixing of the precursor mixture is promoted upon the migration of alcohol from the ternary mixture to an ambient phase using microfluidics. This process is called Solvent Transfer Induced Phase Separation or STrIPS. To illustrate the STrIPS process a ternary phase diagram is used. This diagram gives a graphical representation of the relationship between the phases of the three-component system at constant temperature and pressure. Three regions can be assigned in the phase diagram, based on the thermodynamic stability. The thermodynamic stable phase or the mixed phase is located above the binodal line. Here the Gibbs free energy is minimal, and the mixture is stable to local fluctuations. Below the Binodal line there is a meta-stable phase, where the system is meta-stable to local fluctuations and a nucleation barrier has to be overcome for the formation of a second phase. Then there is the thermodynamic unstable phase located below the spinodal line. Here the Gibbs free energy is maximal and the system is unstable to local fluctuations. There is no need for a nucleation barrier to form a second phase and, uniform phase separation leads to spinodal decomposition. [36,37] The tie-lines link two points on the binodal curve that represent the composition of the two phases (water rich and oil rich) that are generated upon phase separation. The critical point is located at the intersection of the binodal and spinodal line. To arrest a spinodal structure with STrIPS involves a ternary precursor mixture close to the critical point to ensure phase separation occurs via spinodal decomposition.[35]

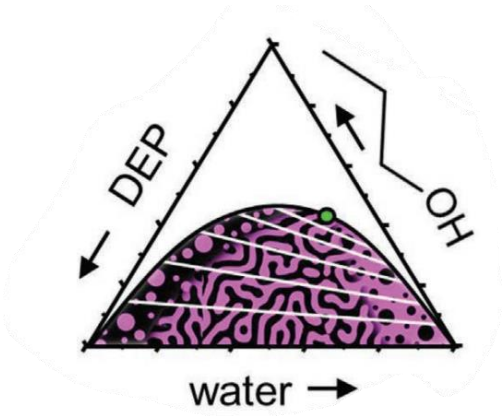

***Figure 7.** Ternary phase diagram of Diethyl phthalate (DEP), 1-propanol and water. The green dot represents the critical point. Image is taken from Khan, M. et al (2022)[36]*

3. Materials and Methods

The table below summarizes all the chemicals used during experiments:

Tabel 1. List of chemicals

Chemicals	Abbreviation	Grade	Supplier	Type of substance
Diethyl Phthalate	DEP	>99%	Acros Organics	hydrophobic liquid / oil
n-Hexane	X	HPLC	Biosolve	hydrophobic liquid / oil
octadecyl(trichloro)silane (OTS)	OTS	X	ChemCruz	Silane
Ludox TMA	TMA	34 wt. %	Grace	Nano-particles
Hexadecyltrimethylammonium bromide	CTAB	>99%	Sigma	Surfactant
Methelyne Blue	X	X	Sigma	Fluorescent Dye
Rhodamine 110 Cl	X	X	Sigma	Fluorescent Dye
Mineral oil	X	X	Sigma-Aldrich	hydrophobic liquid / oil
Tetraethyl orthosilicate (TEOS)	TEOS	>99%	Sigma-Aldrich	Silane
1-Propanol	X	>99.5%	Sigma-Aldrich	Solvent
Fluorescein Sodium salt	Fluorescein	X	Sigma-Aldrich	Fluorescent Dye
9-diethylamino-5H-benzo[a]phenoxazine-5-one	Nile red	X	Sigma-Aldrich	Fluorescent Dye
Polyethylene glycol 200	PEG200	X	Sigma-Aldrich	hydrophilic liquid
dodecane	X	mixture of isomers	thermo scientific	hydrophobic liquid / oil
Glycerol	X	>99%	thermo scientific	hydrophobic liquid / oil
Toluene	X	>99%	thermo scientific	hydrophobic liquid / oil
n-Hexadecane	X	99%	thermo scientific	hydrophobic liquid / oil
octadecyl(triethoxy) silane	X	98%, n-isomer	Santa cruz biotechnology	Silane

3.1 Precursor mixture optimization

Precursor mixtures were prepared with different concentrations of particles, salt and surfactants:

For the 40wt% Ludox TMA, 50 mM NaCl samples, 60g of Ludox TMA 34wt% was concentrated in a rotary evaporator at 60°C and 145mbar for 12 minutes. The concentrated TMA solution was centrifuged for ten minutes at 3500 RPM. The pH was adjusted to 2.9 by adding 1M of HCL dropwise.

For the 40wt% Ludox TMA, 28 mM NaCl samples, 60g of Ludox TMA 34wt% was concentrated in a rotary evaporator at 60°C and 145mbar for 12 minutes. The concentrated TMA solution was centrifuged for ten minutes at 3500 RPM. The concentrated Ludox TMA was than dialyzed in a 4L beaker filled with 3L water with 50mM NaCl at pH = 2.9.

For the 34wt% Ludox TMA, 50 mM NaCl samples, The pH of 60 g of Ludox TMA 34wt% was adjusted to 2.9 by adding 1M of HCL dropwise. NaCl was added until 50mM NaCl was reached.

For the 34wt% Ludox TMA, 28 mM NaCl samples, the pH of 60 g of Ludox TMA 34wt% was adjusted to 2.9 by adding 1M of HCL dropwise

The weight fraction was determined by heating 100 µL of the dispersion in an aluminium cup for five minutes at 150 °C followed by one minute at 300 °C at a heating plate and measuring the weight loss. A stock solution of 50wt% glycerol /1-propanol was prepared. Additionally a 200mM CTAB stock solution was prepared by weighing 0,3645g CTAB and adding five mL 1-propanol. The mixture was vortex mixed and heated to dissolve all the CTAB, if necessary ultrasonication was used. Three fractions were prepared: The water fraction, consisting of 34/40wt% (28/50 mM NaCl) Ludox TMA in water at pH = 2.9 ; the Oil fraction consisting of Diethyl Phthalate (DEP) ; and the Solvent fraction consisting of 50-60 mM CTAB in 1-propanol. The precursor mixtures for bijels were prepared by combining the water, oil and solvent fraction in a volumetric ratio of 50:7:43, respectively. The mixture was vortex mixed and sonicated in a heat bath for a few minutes to ensure complete homogenization.

3.2 Single flow microfluidics

A 50µm (ID) capillary was inserted in a one mL pipette tip, ensuring that approximately 1cm of the capillary protruded from the small end of the pipette tip. A droplet of Norland Optical Adhesive 81 was deposited inside the pipette tip and cured. The pipette tip was sealed at the bottom leaving only the capillary as the opening. An extrusion container was fabricated by cutting a 40ml vial at approximately 3 cm. The upperpart was glued onto a #1.5 microscope slit (0.17 mm) with fast-curing five minute epoxy glue, and left to harden.

The extrusion container was filled with toluene, and precursor mixture was pipetted into the toluene using the prepared tip. The toluene was subsequently replaced for hexane and mixed, this was done twice before the hexane was replaced by a saturated solution of Nile red in hexane. The bijel fibers were characterized using scanning laser confocal microscopy.

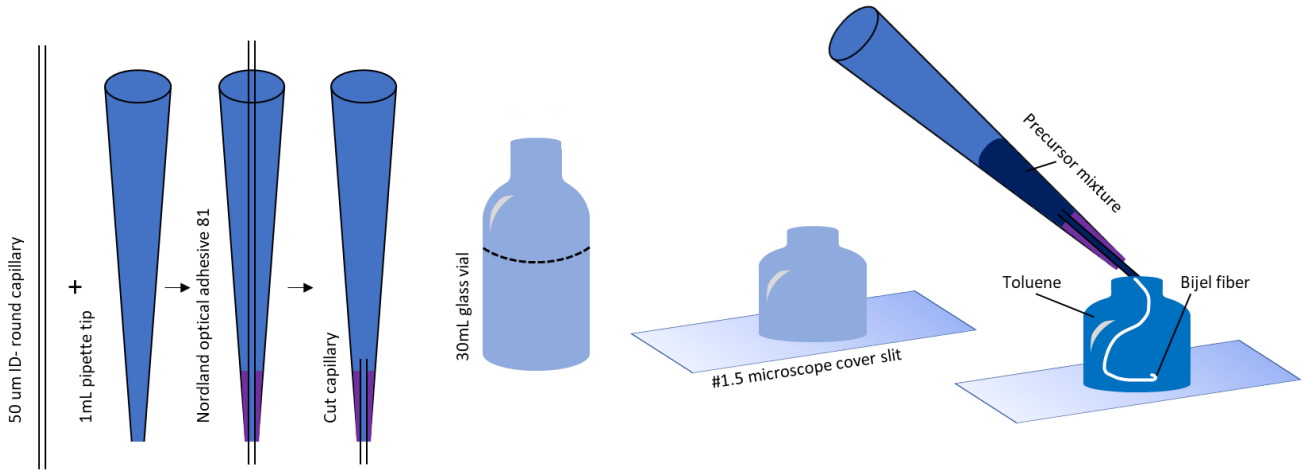

Figure 8. *Bijel production using single flow microfluidics*

3.3 Double flow microfluidics

A 300µm (ID) and a 50µm (ID) round capillary were scored at approximately 5 cm. Similarly, a 100µm (ID) square capillary was scored at approximately 3 cm. Fast-curing 5-min epoxy glue was used to attach the 300µm capillary to a microscope slide, where the capillary protrudes from the slide for approximately 2,5 cm. A droplet of Norland Optical Adhesive 81 was added to the outside of the 50µm round capillary and inserted into the 100µm square capillary and the glue was cured. The assembled capillaries were then inserted in the 300µm capillary and concentric alignment was ensured. With epoxy glue the alignment was pinned. Three 19/20 gauge dispensing needles were used for the inlet and outlet channels. For the flushing channel, the plastic of the dispensing needle was completely

removed using a razor blade. To create the ternary inlet channel, two grooves were cut in the plastic of the dispensing needle in a 90-degree angle. The flushing needle was aligned at 90 degrees with the 50µm capillary end, and the ternary inlet channel was placed on top and sealed with epoxy glue. To create the continuous phase inlet, two grooves were cut in a 180 degree angle in the plastic of a dispensing needle, which was placed at the end of the 300µm capillary and sealed with epoxy glue. After the glue was dry (after 1 hour of 50 degrees in the oven, or letting it stand overnight) a hydrophobic coating was applied to the capillaries interior, this was done by flushing the device with a 3wt. % OTS solution in mineral oil. At 1 ml/h the OTS solution was pumped through the device while it was being heated with a hairdryer. The device was flushed with hexane after approximately 5 minutes to stop the reaction.

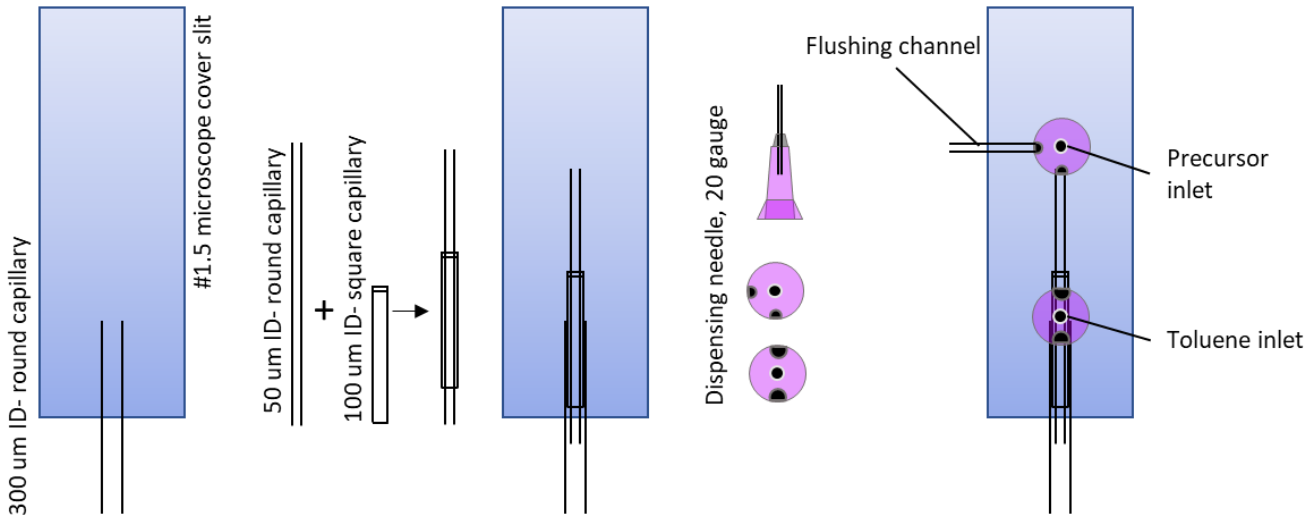

***Figure 9**. Double flow microfluidic device*

3.4 Bijel printing and post processing

Extrusion containers were constructed by sawing a glass tube into small segments (30cm * 40cm * 5cm) (l*w*h). With epoxy glue the segments are glued upon #1.5 microscope slits. A 5 ml syringe was filled with the ternary precursor mixture and placed in a syringe pump. Additionally a 20ml syringe was filled with toluene and added to a second syringe pump. The precursor mixture and toluene were connected to the inlets of a microfluidic device using G19/G20 tubing. The device was mounted on a custom-built Lego printer controlled by a Lego Mindstorms control brick. Extrusion containers are placed under the printer. Continuous bijel fibers were printed by varying the ternary flow speed between 1-2 ml/h and the continuous phase flow speed between 5-6 ml/h. The device was moved through the container using the control brick.

After printing the fibers in the extrusion containers, the fibers were washed with mineral oil three times. Then the containers were filled with approximately 5ml of 3wt % TEOS solution and mixed for even distribution, after 24h the TEOS solution was removed, and washed once with mineral oil. Alternatively the containers were filled with 1.5wt% TEOS solution in mineral oil with 48 hours reaction time. The fibers were washed again with mineral oil, before the addition of different concentrations of OTS in mineral oil for different reaction times (0.5, 1.0, 1.5 wt% OTS for 2 hours and 0.5wt% for 30,90,150 and 240 min). After OTS treatment the fibers were washed with hexane three times, followed by three washing steps with 1-propanol. After that the fibers were left in 1-propanol overnight, to remove all the CTAB. Finally the fibers were washed once more with 1-propanol. All washing steps were done extreme carefully, with the intention for minimal displacement of the bijel fibers. The containers were tilted slightly forward and the liquids were removed from the right corner

of the container by using a 2.5ml plastic pipette. The fresh liquids were added to the left corner of the container with a 2.5ml plastic pipette. Then mixing was done carefully by removing liquids from one corner to the opposite corner and letting it stand for a few minutes.

To check the success of the CTAB washing steps, fluorescein sodium salt in water (pH= 7) was added to containers with: TEOS treated, 1-propanol washed and dried bijel fibers ; TEOS treated, 1-propanol washed followed by a 1M HCl/ Ethanol washed, dried bijel fibers; OTS treated, 1-propanol washed and dried bijel fibers. The same procedure was executed with Rhodamine 110cl in water (pH=7).

3.5 Reconstitution

The dried bijel fibers were cut at the edges. Droplets of nile red in hexadecane were added at midsection of the fibers. Droplets of nile red in PEG200 were added to the cut end of the fibers. Alternatively containers were completely filled with nile red in hexadecane whereafter droplets of nile red in PEG200 were added in the liquid at the end of the cut fibers. The samples were analysed using scanning laser confocal microscopy

3.6 Characterization

Confocal characterization was done using the Leica Stellaris 5 scanning laser confocal microscope. Two excitation sources were used: the 488nm Optically Pumped Semiconductor Laser and the 561nm Diode Pumped Solid State Laser. Freshly printed bijel fibers were analysed using a water objective: HC PL APO CS2 63x/1.20 WATER (n=1.33). For the reconstituted bijel fibers a glycerol objective was used: HC PL APO CS2 63x/1.20 GLYC (n=1.45)

For Scanning Eectron microscopy (SEM) analysis, dried bijel fibers were stuck on a SEM sample stub. This is done making sure part of the fibers were facing upwards to be able to monitor the internal structure of the fibers. A 7nm platinum layer was sputter coated onto the fibers . The samples were analyzed using the Phenom Pro Desktop SEM, with electron optical magnification range of 160-350.000x and a resolution of ≤ 6 nm Secondary Electron detector and ≤ 8 nm Backscattered Electron Detector.

4. Results and discussion

4.1 Bijel synthesis and precursor optimization

As bicontinuous emulsion gels are used as a template for a porous janus material in this project, control over the bijel structure is essential. Bijels are synthesized by extrusion of a ternary precursor mixture to an ambient toluene phase. The composition of this precursor mixture has great impact on the final bijel morphology. Here we kept the ratio between water and oil fixed to be near the critical point on the binodal curve. However the mixture also contains particles, surfactants and salt. To investigate the influence of these constituents, parametric studies concerning the NaCl and CTAB concentration as well as the weight percentage of nanoparticles were performed. Quantitative analysis of bijel fibers is difficult because although bijels share the same fundamental characteristics of intertwined oil and water channels, each individual bijel fiber displays unique features. With confocal microscopy we can however identify certain common features and trends qualitatively.

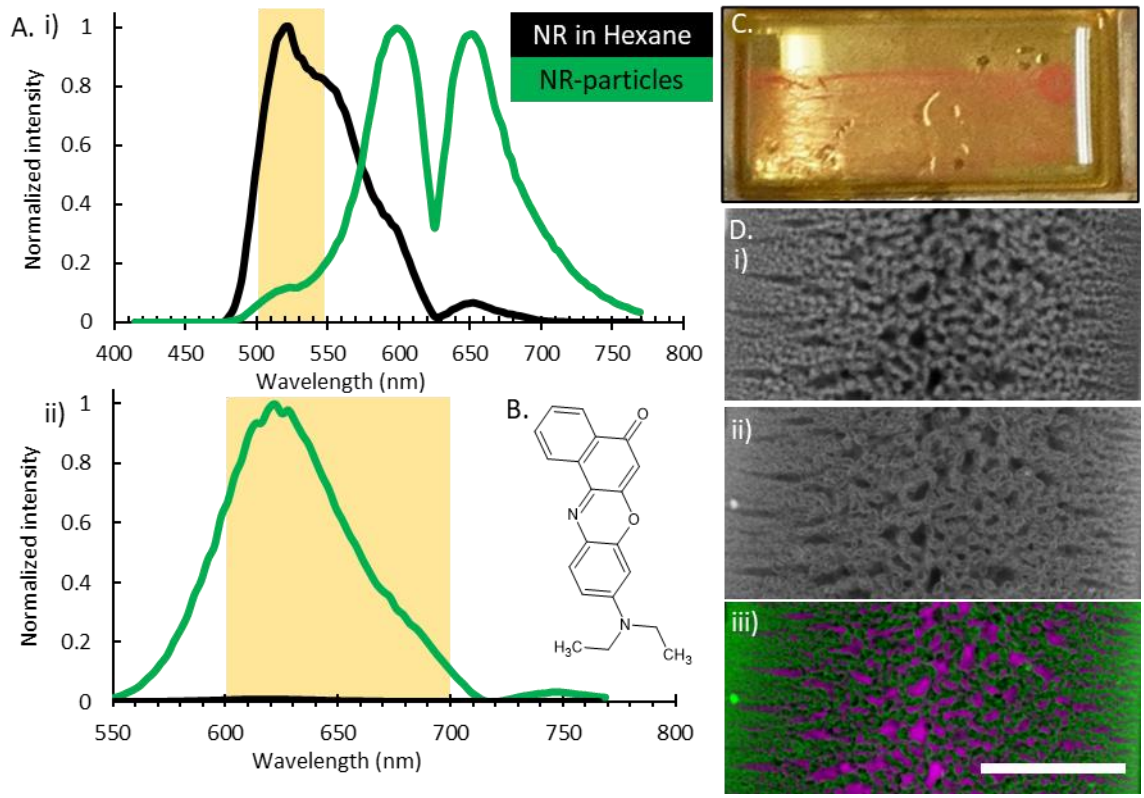

Figure 10. *Bijel imaging* ***A.*** *Emission bands of NR in hexane (black) and NR-particle interaction (green), with highlighted areas representing used emission range for i) 488nm excitation, ii) 561nm excitation.* ***B.*** *Nile Red chemical structure.* ***C.*** *Bijel fibers submerged in NR in hexane* ***D.*** *i) Oil signal 488 nm, ii) particle signal 561nm, iii) composite of I + ii with: oil in black, particles in green, water in magenta. The scale bar indicates 20µm*

Freshly printed bijel fibers are washed with hexane to replace all the toluene with hexane. Nile red (NR) is introduced to the bijel fibers by exchanging the hexane with a saturated NR in hexane solution (10.C). NR is a neutrally charged dye (10.B) that solves well in aliphatic liquids and has low solubility in water where non-emissive dimers are formed. Due to the solvatochromic properties of this dye the NR-particle interaction yields a different emission profile than the NR in hexane. This change in fluorescence behaviour is due to the presence of CTAB that causes strong adsorption of NR and changes the local polarity. By using two different laser excitation wavelengths and emission ranges, this difference can be exploited to differentiate between particles and the oil phase, as is shown in figure 10.A. The fluorescence signal of NR in hexane however is relatively weak in comparison with

the NR-particle fluorescence signal, therefore a much higher laser intensity is used to monitor the oil phase. For optimal image quality glycerol (n=1.40) is added to the water (n=1.33) phase of the ternary precursor mixture, this ensures refractive index matching with hexane (n=1.37). When the difference in refractive index is too large, the multiple aberrations of the direction of light cause a significant reduction of image quality. Figure 10.D shows the confocal micrographs of the equatorial plane of a freshly printed bijel fiber, where i) and ii) show the fluorescence signal for 488nm and 561nm excitation respectively. In iii) the channels are combined, where the water phase is false coloured in magenta.

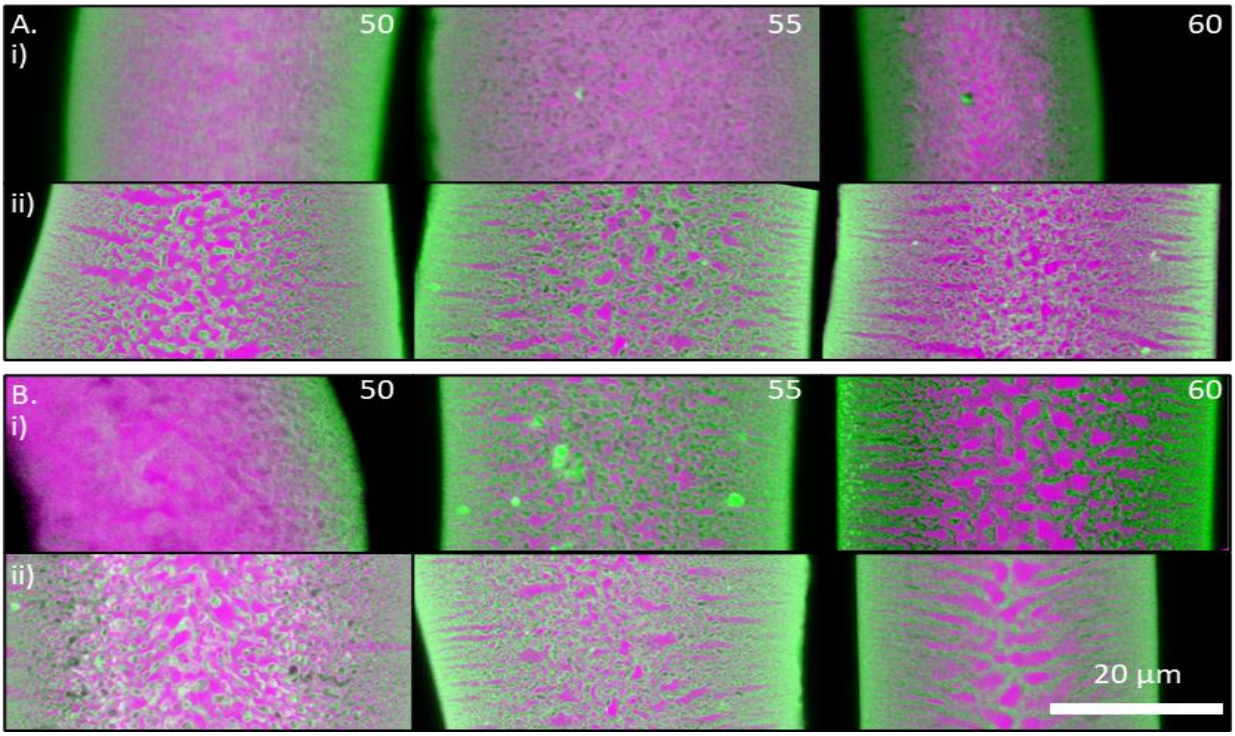

Figure 11. *Confocal micrographs of bijel fibers prepared with a precursor mixture containing* ***A.*** *40wt% nanoparticles with* ***i)*** *50 mM NaCl and 50-60 mM CTAB* ***ii)*** *28 mM NaCl and 50-60 mM CTAB.* ***B.*** *34wt% nanoparticles with* ***i)*** *50 mM NaCl and 50-60 mM CTAB* ***ii)*** *28 mM NaCl and 50-60 mM CTAB. The scale bar indicates 20µm*

Precursor mixtures were prepared with hexadecyl-tri-ammonium bromide (CTAB) concentrations ranging from 50-60 mM, two different concentrations of particles and with and without the addition of NaCl. All the mixtures were extruded into toluene using a single flow device, with a capillary size of 50µm. The confocal micrographs of the produced bijel fibers are shown in figure 11.A (40wt% particles) and 11.B (34wt% particles). Although the micrographs were taken at the equatorial plane of the fiber, the diameter of these fibers ranges from 30 µm – 80 µm. This can be accounted for by the single flow devices that are used to produce the bijel fibers. The pressure applied to the pipette is not the same everywhere because it was done by hand. Also, the capillaries where not hydrophobically coated, this caused the precursor mixture to clog the capillaries over time. Despite this lack of restraint, this technique offers a quick method to investigate the interior bijel structures obtained for different precursor mixtures, and although the robustness is limited certain trends can be observed.

The amount of aggregated particles, as displayed by bright green spots in the micrographs are present more often at high CTAB concentrations, predominantly for the samples with a higher salt concentration. Secondly, the amount of radially aligned channels, expanding from the centre of the fiber to the periphery are increased when the concentration of CTAB is increased. Many factors influence the formation and stabilization of the bicontinuous network of two interwoven liquid channels during STrIPS, such as: solvent flow rate, precursor mixture flow rate, solvent partitioning

rate, interface jamming. We assume that the effect of salt and CTAB in the precursor mixture both have the most impact on the surface properties of the nanoparticles and therefore mostly affect the interfacial jamming process. The presence of NaCl shields the effective charge of the negatively charged nanoparticles, this reduction in charge leads generally to a more hydrophobic surface[37], which is also achieved upon increasing the CTAB concentration.

The hydrophobicity of the nanoparticle surface has great influence on the attachment energy of the particles to the interface. Neutral wetting of the particles yields the highest attachment energy and an increase in hydrophobicity not only leads to a lower attachment energy, but also the preferred emulsion stabilization is changed. More hydrophobic particles prefer the stabilization of w/o emulsions. Both these effects may impact the frequency of radial channels observed in the bijel structure. However kinetic effects also could play a significant role, as aggregation of the particles takes place, the size and mass of the effective particles increases resulting in a lower movement of the particles and the spinodal domains are slower stabilized and are allowed to coagulate more. Due to the many-sided STrIPS process, it is hard to draw definite conclusions regarding the impact of the precursor mixture composition on the final obtained bijel structure. Most importantly we show that bicontiunuous structures can be obtained without the addition of salt or concentrating the particles. (the ludox TMA particles are supplied at 34wt%, 28mM salt.) Before the production of bijel fibers for post treatment the precursor mixture is always varied in CTAB concentration to select the mixture where the optimal structure is obtained.

4.2 bijel post processing

The optimized precursor mixture is used for printing of bijel fibers in multiple containers with a double flow microfluidic device. The following post-processing treatments are executed and will be discussed in the following chapters, TEOS treatment for crosslinking the particle scaffold, OTS treatment for the selective hydrophobization, where the OTS weight percentage is varied (figure 12.)and with a variation in reaction time (figure 13.)

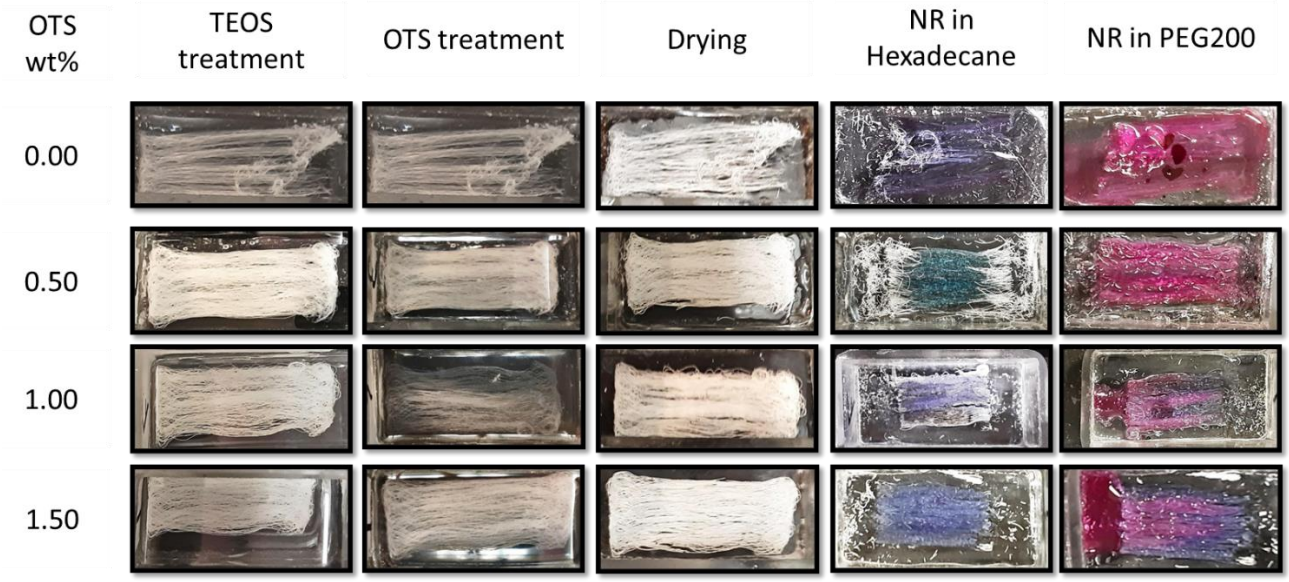

***Figure 12**. Bijel post processing steps, where 24hours TEOS treatment and 2 hours of OTS treatment were used, the reconstitution experiments were executed using droplets of hexadecane on the midsection, followed by the addition of PEG200 to the fibers end.*

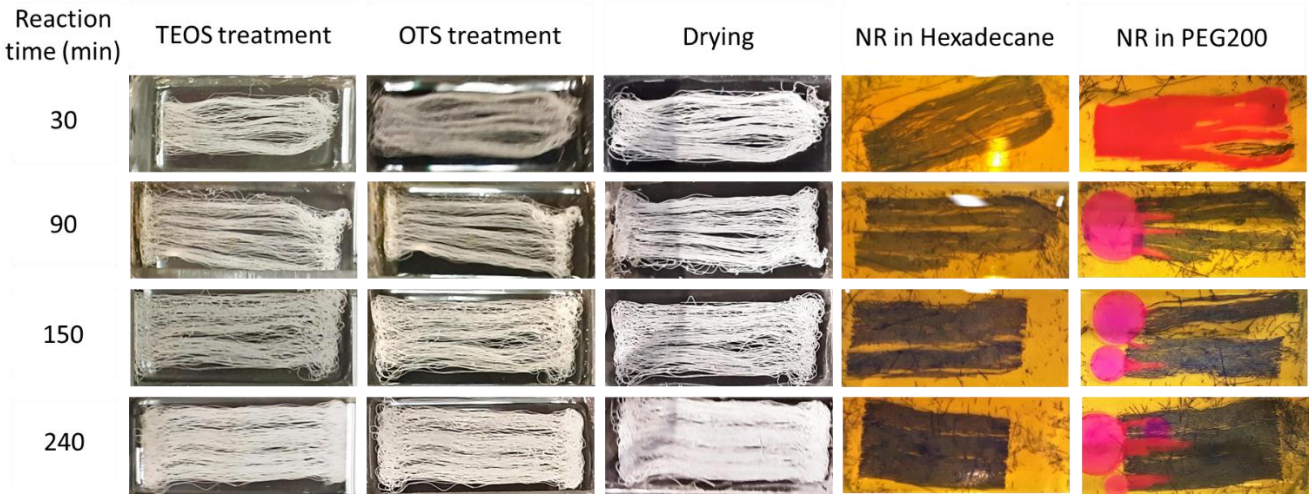

***Figure 13**. Bijel post processing steps, where 24hours TEOS treatment and 0.5wt% of OTS treatment was used, the reconstitution experiments were executed by completely submerging the fibers in hexadecane, followed by the addition of PEG200 to the fibers end.*

4.2.1 Tetraethyl orthosilicate (TEOS) treatment

Although the nanoparticles inside bijels are fixed at their position, upon removal of the liquids the structure falls apart. To prevent the degradation of the bijels and increase the resistance to mechanical stresses, the nanoparticle scaffold is reinforced with additional silica. This is done by means of crosslinking the system with Tetraethyl orthosilicate (TEOS). TEOS is administered via the oil phase and locally fuses the nanoparticles via silica deposition. The reaction is acid catalysed (water pH= 3 used in the precursor mixture) and runs at standard conditions. The mechanism contains four steps that are schematically represented in figure 14. First the ethoxy groups of TEOS are hydrolysed, followed by condensation to oligomers. The OH groups at the nanoparticle surface then hydrogen bond with the oligomers. Lastly covalent linkage takes place between the organo-silane and the nanoparticle surface. The last three steps don't necessarily occur in that order, ultimately TEOS treatment creates a branched polysiloxane network reinforcing the nanoparticle scaffold.

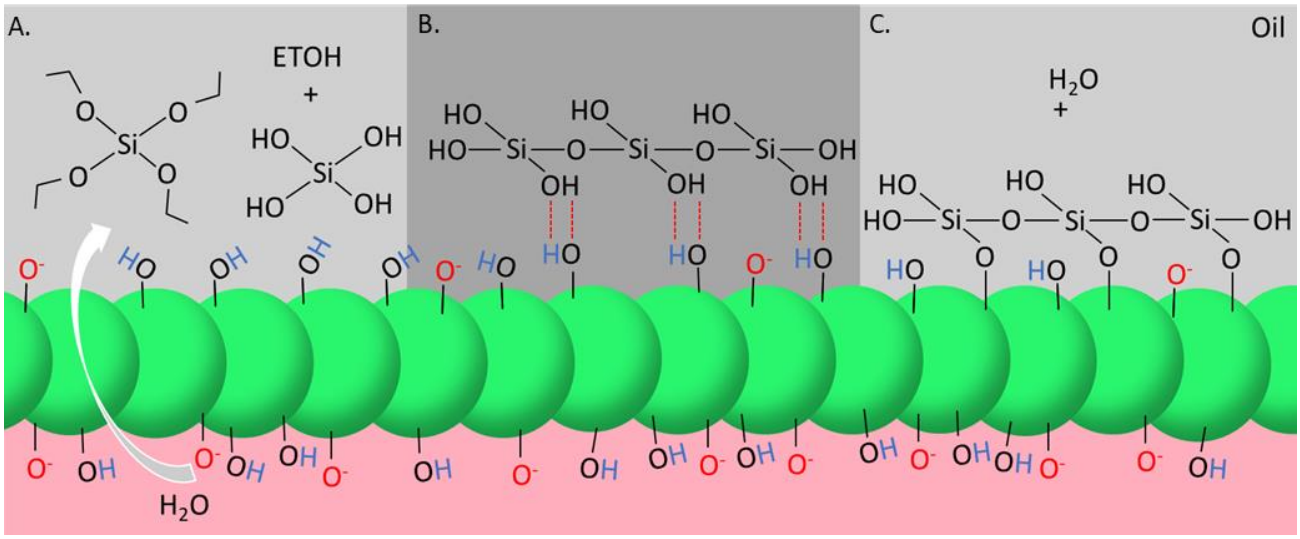

***Figure 14.** Schematic representation of the crosslinking mechanism. **A.** Hydrolysis of TEOS **B.** Polymerization and Hydrogen bond coordination **C.** Covalent binding to the nanoparticle scaffold.*

After TEOS treatment, the fibers can be washed to remove all the liquids without the particle network degrading. To visualize the interior structure of TEOS treated bijel fibers, the fibers are cut with a razor blade and analyzed using Scanning Electron Microscopy (SEM). A cross section of a successfully TEOS treated bijel fiber is shown in figure 15.A i) The spongelike structure shows the interconnected pore system remains intact. The TEOS treatment however doesn't seem to have a consistent effect on the bijels. In 15.A ii) The same procedure of 3wt% TEOS in mineral oil for 24 hours is executed, however the interior structure is collapsed. Another major problem during TEOS treatment is the replacement of the previously water filled pores in bijels with oil, which is sometimes referred to as oil-leakage.[38] During treatment this can be observed as the fibers start to get transparent. When water is present inside the fibers there is a refractive index mismatch between water/glycerol (n=1.37) and particles (n=1.45), this gives the fibers a bright white colour (figure 15.B,i). However during TEOS treatment, mineral oil (n=1.47) can start to displace the water, and the refractive index becomes similar for all constituents, and the fibers become transparent.(15.B,ii). This can also be observed with confocal analysis. Where the untreated fibers display a clear separation between the oil and water phase (15.C,i), the TEOS treated fibers show a water phase that is locally replaced by oil (15.C,ii). Lowering the wt% TEOS used and increasing the reaction time (1.5wt%, 48h) seem to improve the bijel stability. (15.C,iii)However it is hard to make conclusive remarks about this, since oil-leakage seems to happen in a randomly manner. The treatment of the fibers requires a lot of washing steps, that are currently done by replacing liquids with a pipette. Although this procedure is handled with the uttermost caution not to displace the fibers, the washing procedure could be a major reason for the presence of oil leakage. The problems during TEOS treatment create major implications on the following in-situ surface treatment of the bijels, as the reactants are delivered inside the bijel via the oil-phase. Better understanding of this problem could improve the control over the entire process.

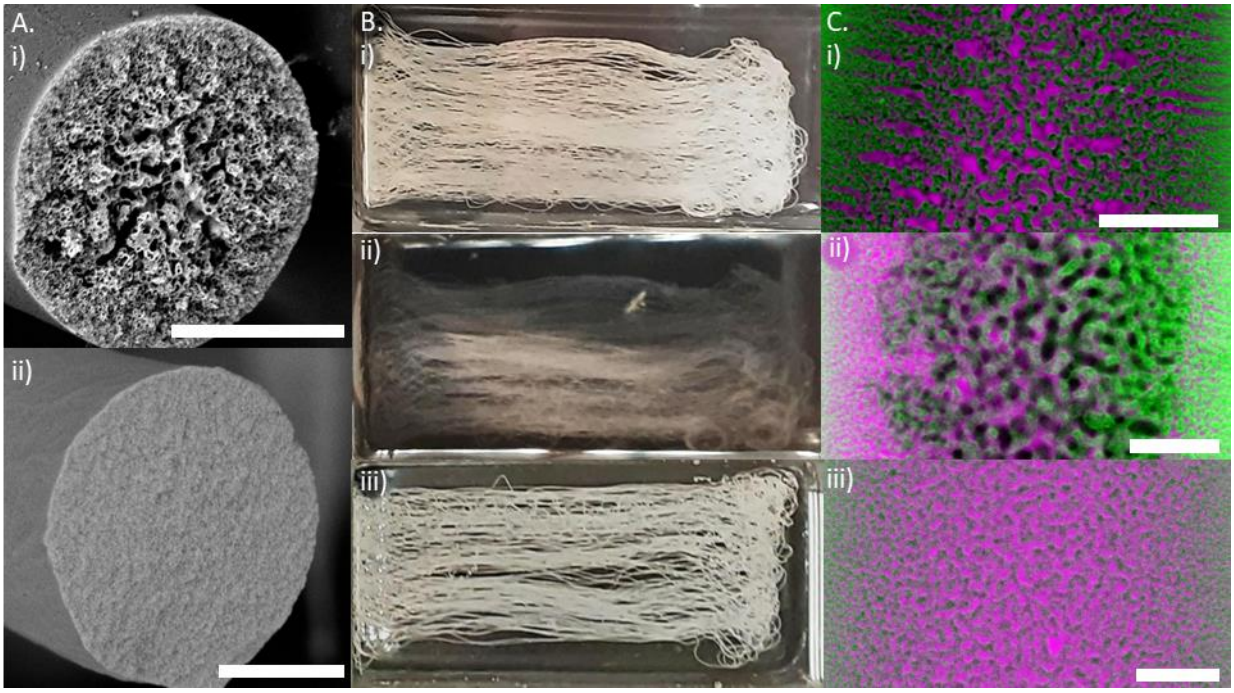

***Figure* 15.** *TEOS treatment **A. i)** Bijel fibers in Toluene **ii)** Bijel fibers in mineral oil after 24h 3wt% TEOS treatment **iii)** bijel fibers in mineral oil after 48 hours 1.5wt% TEOS treatment **B.** Confocal micrographs of **i)** untreated bijel fiber **ii)** bijel fibers after 24h 3wt% TEOS treatment **iii)** Bijel Fibers after 48h 1.5wt% TEOS treatment **C.** SEM images **i)** collapsed fiber **ii)** successful TEOS treated fiber. The scale bars indicate 20um*

4.2.2 Octadecyl trichlorosilane (OTS) treatment

Following successful reinforcement, the bijel interior is treated with Octadecyltrichlorosilane (OTS) for the selective hydrophobization of the oil-phasing part of the nanoparticle scaffold. The oil phase of the system is changed for an OTS solution in mineral oil. The selectivity is thought to be achieved because the silanes are administered via the oil-phase while the water remains in place. The mechanism is similar to that of TEOS treatment, the silanes are covalently bonded to the particles by hydrolysis, condensation, hydrogen bonding and covalent linkage of OTS to the nanoparticle scaffold , which is schematically depicted in figure 16. Hydrophobicity is achieved due to the exchange of silanol group with silanes containing aliphatic tails.

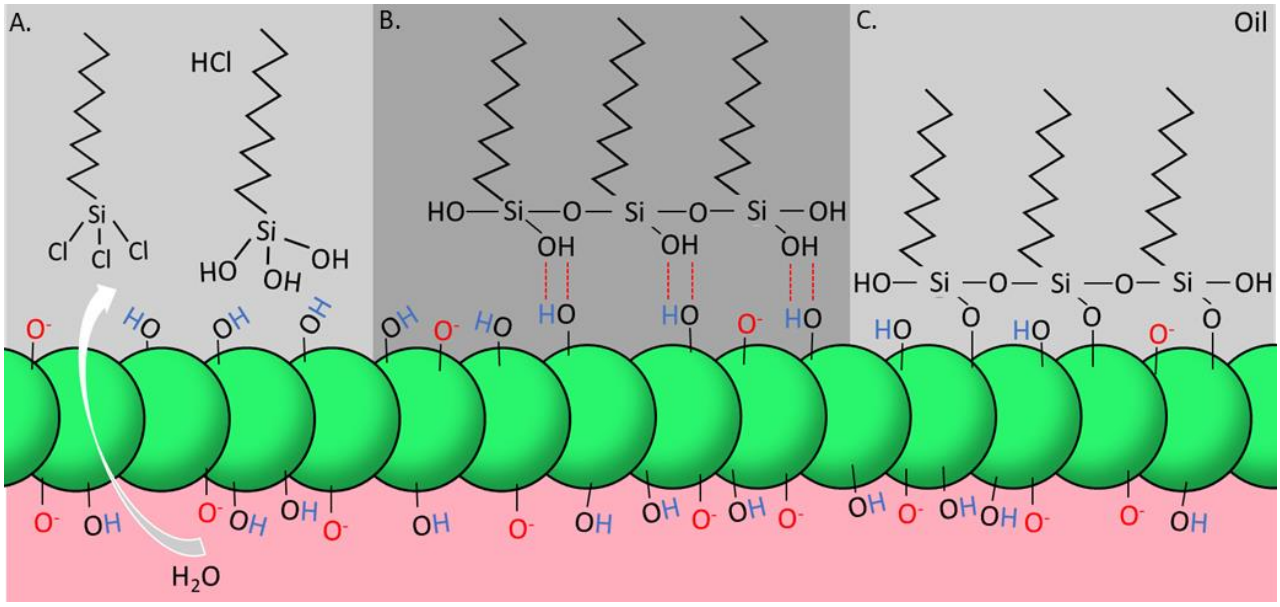

Figure 16. *schematic representation of selective hydrophobization treatment with OTS.* ***A.*** *Hydrolysis of OTS* ***B.*** *Polymerization and Hydrogen bond coordination* ***C.*** *Covalent binding to the nanoparticle scaffold.*

For the OTS-treatment initially concentrations of 0.5 – 1.5 weight percentage are used with a reaction time of 2 hours. The fibers are washed and dried and SEM analysis shows some structural changes that occurred after this treatment (figure 17.). At increasing OTS wt%, the internal channels start to fuse together forming larger domains of particles. The surface of the fibers also undergoes some changes, where after TEOS treatment the surface was relatively smooth, the surface becomes more rough at increasing the OTS wt%, indicating the presence of polysiloxane branching on the surface of the fibers. This is undesirable, since we want to control the reaction to occur at the oil-phasing side of the particles inside the bijel. At 0.5 wt% OTS surface branching is limited, to find the optimal time required for the reaction, 0.5wt% OTS is used and the reaction time is varied between 30 and 240 minutes. The SEM images show the perseverance of the internal structure of the bijels at reaction times up until 240 minutes (figure 18.). The surface roughness increases over time, but the organo-silanes seem to grow in a more equally distributed fashion in comparison with the higher wt% of OTS used as observed in figure 17.

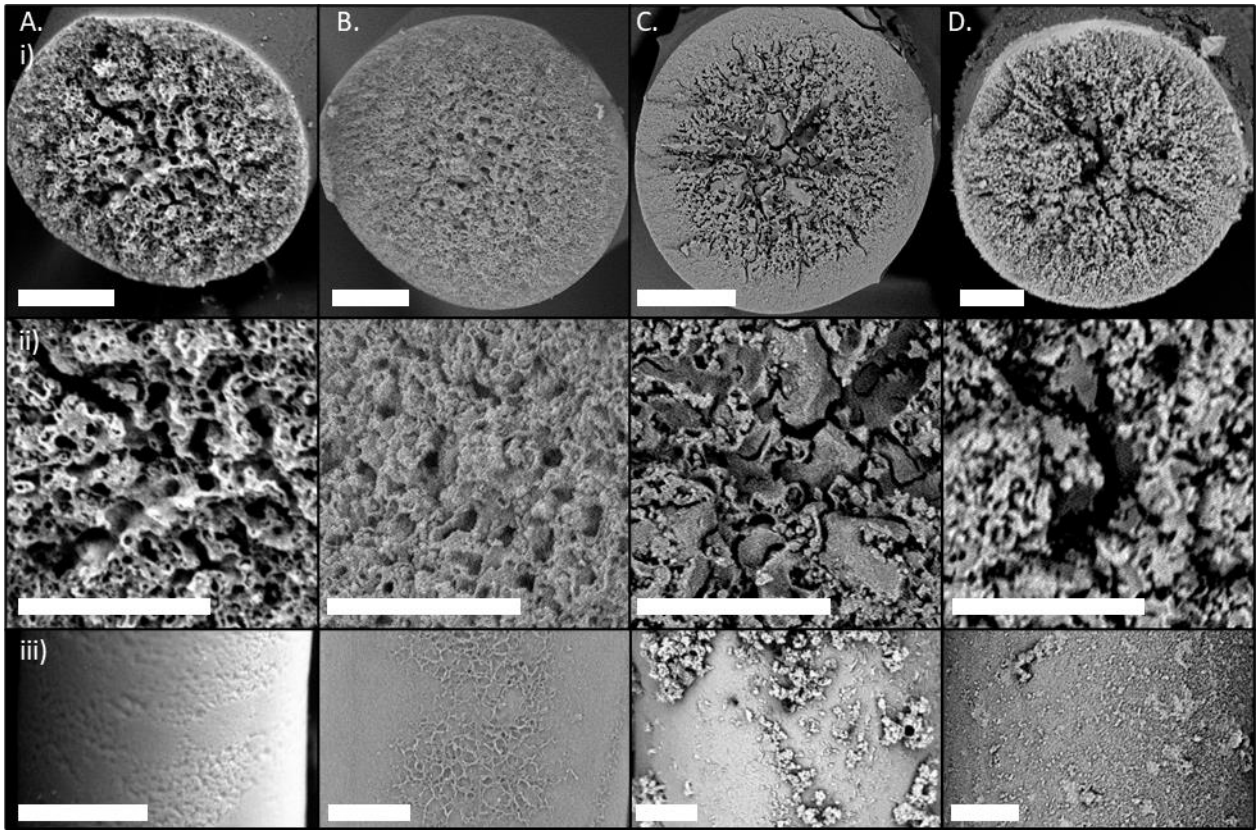

Figure 17. *OTS treated fibers (2h):* ***A.*** *control sample (only TEOS treatment)* ***B.*** *0.5 wt% OTS* ***C.*** *1.0 wt% OTS* ***D.*** *1.5 wt% OTS Different perspectives:* ***i)*** *Cross section* ***ii)*** *magnification bijel interior from cross section* ***iii)*** *Fiber surface*

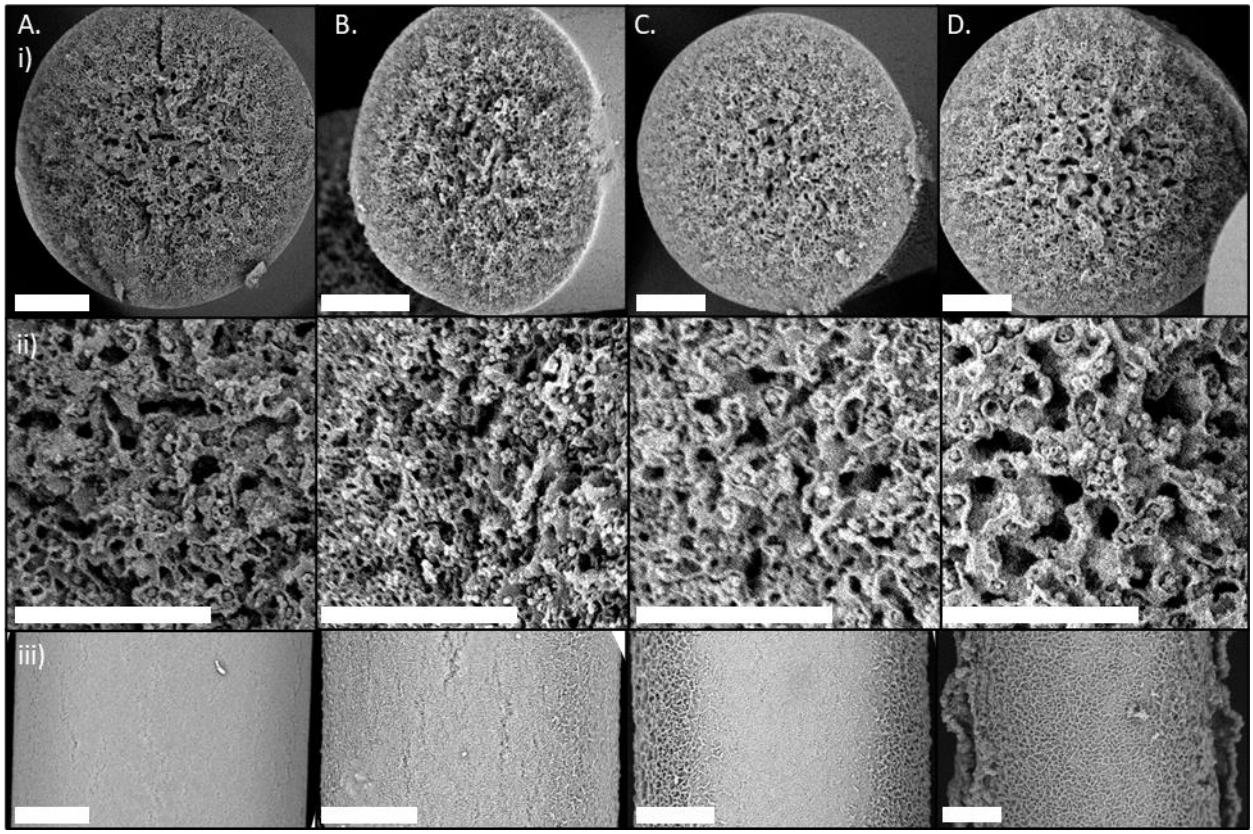

Figure 18. *OTS treated fibers (0.5wt% OTS):* ***A.*** *30 min. reaction time* ***B.*** *90 min. reaction time* ***C.*** *150 min. reaction time* ***D.*** *240 min. reaction time. Different perspectives:* ***i)*** *Cross section* ***ii)*** *magnification bijel interior from cross section* ***iii)*** *Fiber surface*

4.3 Reconstitution

To determine the effectiveness of the hydrophobization treatment, hydrophobic (Hexadecane) and hydrophilic (PEG200) liquids are introduced to the treated bijel fibers (figure 19.), the bijels are reconstituted in this way. NR dissolves well in both liquids and the emission bands allow for good distinction between both phases (figure 19.A). Moreover the refractive index of PEG200 and hexadecane matches very well (1.435 and 1.458 respectively). With confocal microscopy the distribution of the liquids inside the particle scaffold is monitored. The hydrophobic and hydrophilic channels are shown in figure 19.B.

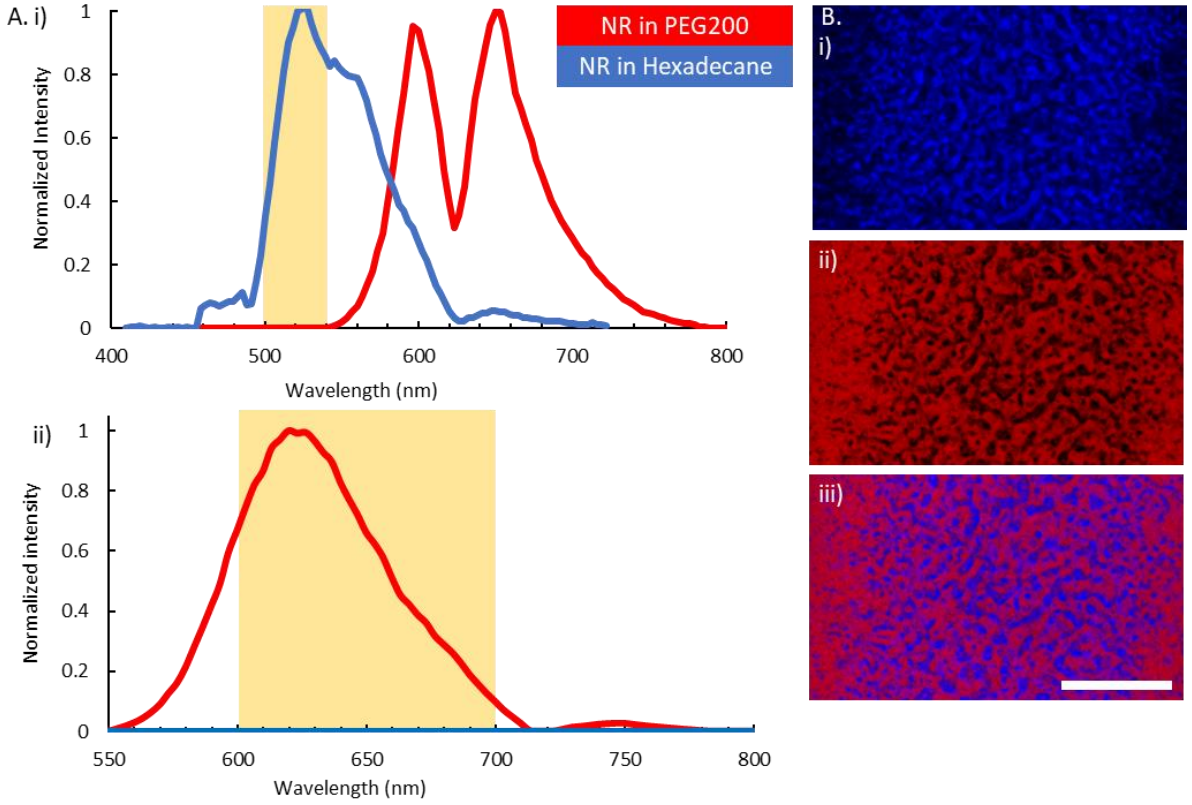

***Figure 19**. Dyes used for reconstitution. **A. i)** Emission bands of NR in hexadecane (blue) and NR in PEG200 (red), with highlighted areas representing used emission range for **i)** 488nm excitation, **ii)** 561nm excitation. **B.** confocal micrograph of **i)** hexadecane signal inside fiber **ii)** PEG200 inside fiber **iii)** combined channels. The scale bar indicates 20µm*

Figure 20.A shows a control sample used for the experiments, the reconstitution of TEOS treated fibers. Interestingly the oil and water channels seem to be selectively filled and the distribution of hexadecane (20.B) is comparable to hexane in freshly printed bijel fibers (20.C). This is unexpected since the TEOS treatment should render the particle scaffold hydrophilic favouring wetting by PEG200 over hexadecane in these fibers that have not yet been OTS treated. The presence of CTAB not being properly removed during the washing steps of the fibers, gives a possible explanation. The potency of the 1-propanol wash to remove CTAB is tested by introducing positively and negatively charged dyes to bijel fibers. At neutral pH the particle scaffold is negatively charged due to deprotonation of silanol groups, the presence of CTAB (cationic surfactant) however allows for co-adsorption of negative ions. This effect is visible for 1-propanol washed fibers submerged in fluorescein salt in water (pH=7) (20.A,i), where the interface between the pores gives a bright signal. The opposite is true when we add a positive charged dye (Rhodamine 110 Cl) to the fibers, now the bright signal at the interface is not present. (20.A,ii) A more rigorous washing procedure with 1M HCl and ethanol removes the CTAB to a higher extent. The signal is now reversed, no signal at the interface for the negative dye (20.B,i) and strong adsorption to the particles with a positive dye (20.B,ii). For 0.5 wt% OTS (2h) treated fibers

there is no strong adsorption of positive or negative dye to the particles indicating a successful surface modification.

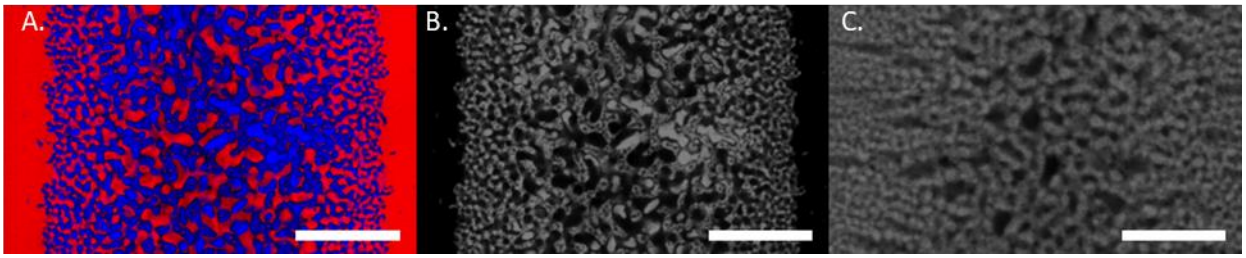

***Figure 20**. Confocal micrograph of **A.** TEOS treated reconstituted bijel fiber with PEG200 (red) Hexadecane (blue). **B.** Isolated hexadecane signal. **C.** Hexane signal of a freshly printed bijel fiber. The scale bar indicates 20µm*

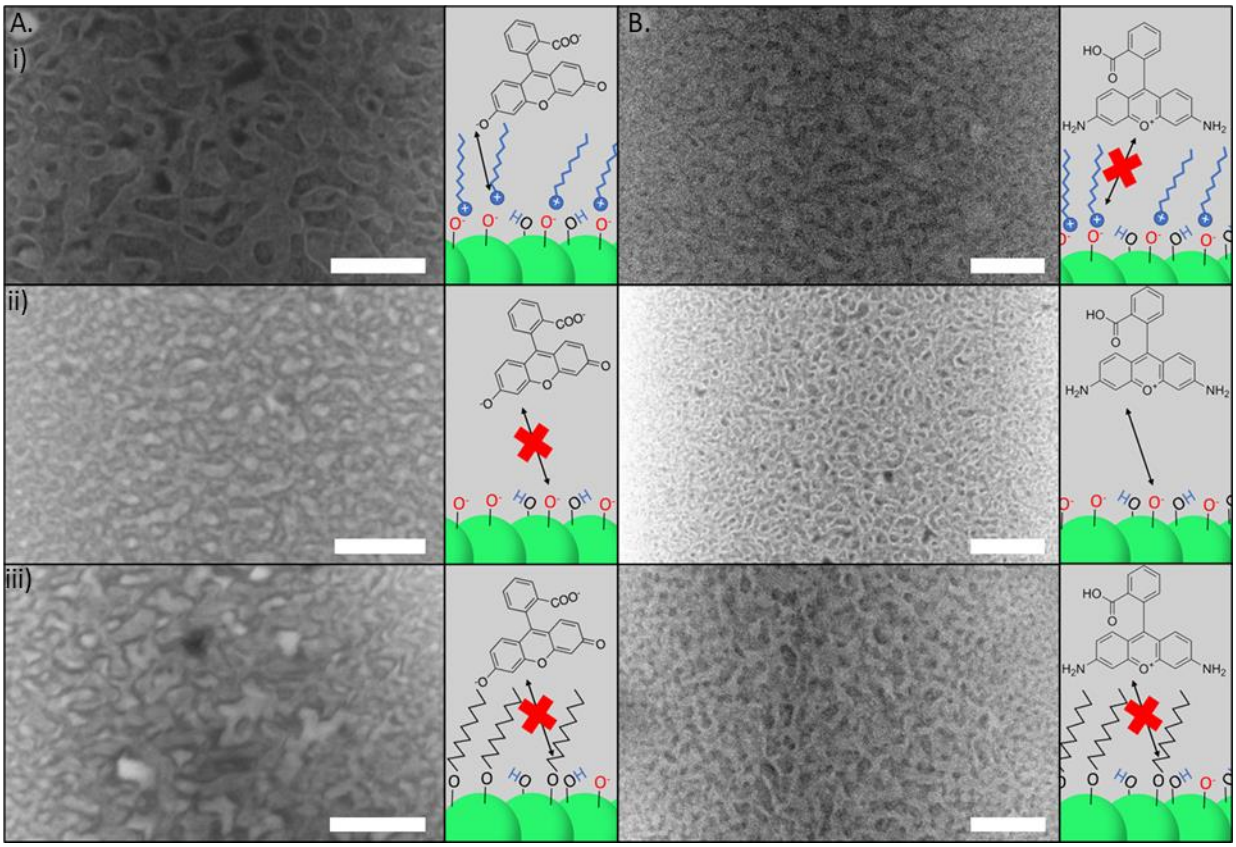

***Figure 21**. Confocal micrographs of washed and dried bijel fibers submerged in **A.** Fluorescein sodium salt in water **B.** Rhodamine 110 cl in water for **i)** TEOS treated and 1-propanol washed bijel fibers **ii)** TEOS treated, 1-propanol washed and HCL/ETOH washed bijel fibers **iii)** TEOS and OTS treated 1-propanol washed bijel fibers. A schematic representation of the particle-dye interaction is displayed on the righthand sight of the micrographs. The scale bars indicate 20µm.*

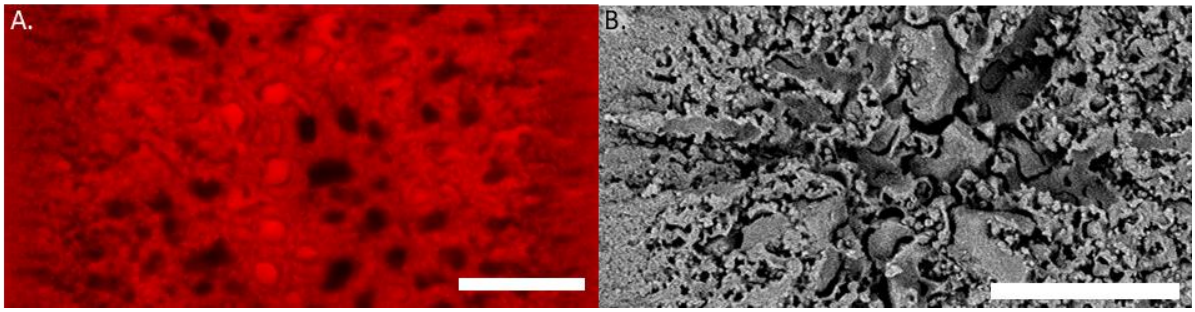

***Figure 22**. 1.5wt% OTS treated bijel fiber with **A.** PEG200 signal of reconstituted fiber **B.** SEM image of particle scaffold interior.*

An other problem, that occurs with the dye system that is used, is the particle-NR emission bands overlap with the PEG200 bands for both excitation energies. As can be seen in figure 22 it is hard to distinguish the particles from the PEG200 signal inside OTS treated bijel fibers. To remedy this problem water is added to PEG200 to increase the hydrophilicity and potentially change the emission profile. Mixtures of NR in different ratios of PEG200 and H2O were prepared. The change in emission bands interestingly depends on the excitation energy used. With 488nm excitation no shift in spectral peak position is observed, however the ratio between the intensity of the two peaks does change upon increasing the water to PEG200 ratio. For 561nm excitation a red shift is observed for the large peak at lower wavelength, while the relative intensity of the second peak decreases upon increasing the H20 to PEG200 ratio. Although we are able to slightly manipulate the emission signal the addition of water to PEG200, it was not enough to distinguish particles and the hydrophilic phase. For this reason the reconstitution experiments were executed with NR in PEG200 without the addition of water and Hexadecane, with the focus on the oil channel.

Figure 23. shows reconstituted fibers for different wt% OTS that is used. And in figure 24 reconstituted fibers for 0.5wt% OTS treated fibers with different reaction times are shown. However it is hard to draw any conclusions from these images. An attempt was made to quantify the amount of oil present inside the pores. The hexadecane signal was binarized and the area occupied with oil was calculated using imageJ. The area does increase upon using a higher weight percentage, 18.78, 29.29 and 45.29 %Area was calculated for the reconstituted 0.5, 1.0 and 1.5wt% treated bijel fibers respectively. When compared with the control sample however these values are all much lower, as the TEOS treated fibers were calculated to occupy 46.47 % Area filled with hexadecane upon reconstitution. For the 0.5wt% OTS treated fibers the area filled with hexadecane showed the opposite trend. 28.85, 25.34 and 20.57 %Area was calculated for the reconstituted 0.5wt% OTS treated samples for 30, 90 and 150 min respectively.

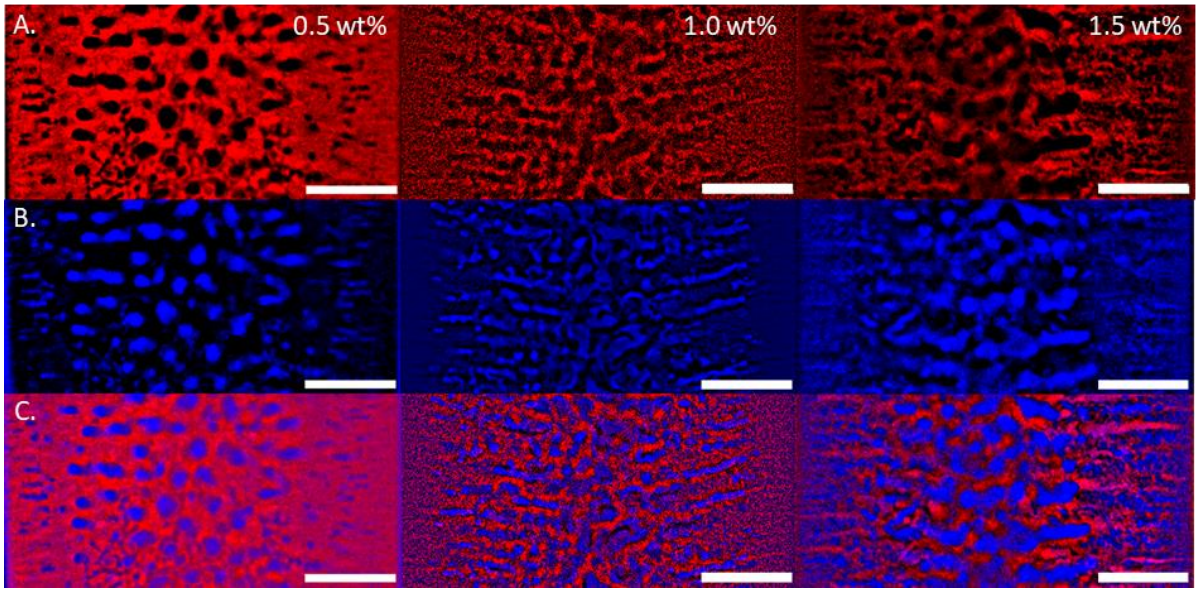

Figure 23*. Confocal micrographs of reconstituted 2 hours, 0.5, 1.0 and 1.5 wt% OTS treated bijel fibers.* ***A.*** *PEG200 signal.* ***B.*** *Hexadecane signal* ***C.*** *Combined channels.*

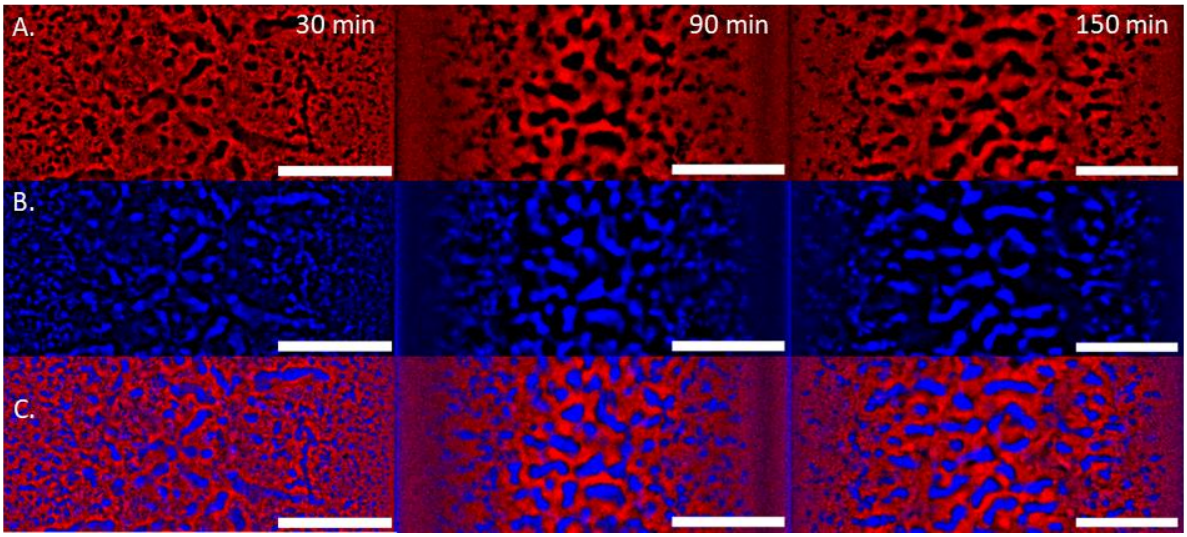

***Figure 24**. Confocal micrographs of reconstituted 30, 90 and 150 min, 0.5wt% OTS treated bijel fibers. **A.** PEG200 signal. **B.** Hexadecane signal **C.** Combined channels.*

5. Conclusions and outlook

During this research we were investigating the possibility of using Bicontinuous interfacially jammed emulsion gels as template for a Janus porous material for the optimization of Hydrogen Fuel cells. With STrIPS bijels were printed and we have showed that precursor mixtures can be prepared containing 34wt% particles without the addition of salt, leading to a faster process, which is useful because precursor preparation is a time demanding process. The bijels were successfully reinforced using TEOS, problems as oil leakage are still present, but the reduction of the TEOS concentration and an increased reaction time seem to have a positive impact on the nanoparticle scaffold stability. The OTS treatment successfully modifies the internal bijel structure as is shown by the charged dye experiments, however at high concentrations of OTS an uncontrolled layer of polysiloxane branches out over the surface of the bijel fibers. Using 0.5wt% OTS in mineral oil gives a higher controlled reaction. The dye system that is used for the reconstitution experiments, gives a good indication of the Hexadecane present inside the pores, the PEG200 however is hard to assign, since the signal overlaps with the NR-particle signal. Overall it is hard to determine the wettability of the pores inside the treated bijel scaffold, but we can say that the interior is somewhat modified and not flood by a single phase during reconstitution.

More control and understanding of the TEOS treatment would be helpful in the future. And for the material to be used as a GDL in a hydrogen fuel cell it is required to improve the resistance to mechanical stresses to a higher extend. Even after successful TEOS treatment, the fibers are very weak and easily collapse when not handled with care.

6. Acknowledgements

I would like to thank dr. Martin F. Haase and dr. Azeem M. Khan for the supervision during this project. I would also like to thank Matthijs for his help with the wettability studies we did, although they did not end up in useful results. The technical assistance from Dominique and Alex is also much appreciated. The group meetings with the Haase group were also nice to discuss issues and practice presentation skills. Lastly I would like to thank FCC for the pleasant work environment.

7. Bibliography

1. Hosseini, S. E. & Wahid, M. A. Hydrogen production from renewable and sustainable energy resources: Promising green energy carrier for clean development. *Renewable and Sustainable Energy Reviews* vol. 57 850–866 Preprint at https://doi.org/10.1016/j.rser.2015.12.112 (2016).
2. O'Hayre, R., Cha, S.-W., Colella, W. & Prinz, F. B. *Fuel Cell Fundamentals*. *Fuel Cell Fundamentals* (2016). doi:10.1002/9781119191766.
3. Navarro, A. J., Gómez, M. A., Daza, L. & López-Cascales, J. J. Production of gas diffusion layers with cotton fibers for their use in fuel cells. *Sci Rep* **12**, (2022).
4. Li, H. *et al.* A review of water flooding issues in the proton exchange membrane fuel cell. *Journal of Power Sources* vol. 178 103–117 Preprint at https://doi.org/10.1016/j.jpowsour.2007.12.068 (2008).
5. Forner-Cuenca, A. *et al.* Advanced Water Management in PEFCs: Diffusion Layers with Patterned Wettability. *J Electrochem Soc* **163**, F1038–F1048 (2016).
6. Forner-Cuenca, A. *et al.* Engineered Water Highways in Fuel Cells: Radiation Grafting of Gas Diffusion Layers. *Advanced Materials* **27**, 6317–6322 (2015).
7. Yan, L. *et al.* Porous Janus materials with unique asymmetries and functionality. *Materials Today* vol. 51 626–647 Preprint at https://doi.org/10.1016/j.mattod.2021.07.001 (2021).
8. Hamilton, E. *Mythology*. Grand Central Publishing. (2011)
9. Yang, H. C. *et al.* Janus Membranes: Creating Asymmetry for Energy Efficiency. *Advanced Materials* **30**, (2018).
10. Casagrande C., Fabre P., Raphaël E., Veyssié M., Janus Beads: Realization and Behaviour at Water/oil interfaces. *Europhysics Letters, Volume 9, number 3.* (1989)
11. Wang, Z., Wang, Y., & Liu, G. Rapid and Efficient Separation of Oil from Oil-in-Water Emulsions Using a Janus Cotton Fabric. *Angewandte Chemie*, *128*(4), 1313–1316. (2016)
12. Lehtinen, M. J., Liu, G., Wu, J., & Pasternak, A. R. O. Antimicrobial Janus Filters that Break Oil-in-Water Emulsions and Separate Oil. *ACS Applied Polymer Materials*, *2*(12), 5851–5863. (2020)
13. Xue, Z. H., Su, H., Yu, Q. Y., Zhang, B., Wang, H. H., Li, X. H., & Chen, J. S. Janus Co/CoP Nanoparticles as Efficient Mott–Schottky Electrocatalysts for Overall Water Splitting in Wide pH Range. *Advanced Energy Materials*, *7*(12). (2017)
14. Cates, M. E. & Clegg, P. S. Bijels: a new class of soft materials. *Soft Matter* **4**, 2132–2138 (2008).
15. Clegg, P. S., & Thijssen, J. H. J. CHAPTER 1: Introduction to Bijels. In *RSC Soft Matter* (Vols. 2020-Janua, Issue 10). The Royal Society of Chemistry.(2008)
16. Di Vitantonio, G., Wang, T., Haase, M. F., Stebe, K. J. & Lee, D. Robust Bijels for Reactive Separation via Silica-Reinforced Nanoparticle Layers. *ACS Nano* **13**, 26–31 (2019).
17. De Gennes, P. G. *Wetting: statics and dynamics*. (1985).
18. Brini, E. *et al.* How Water's Properties Are Encoded in Its Molecular Structure and Energies. *Chem Rev* **117**, 12385–12414 (2017).
19. David w., C. & Reserved, A. R. *David W. Ball-Physical Chemistry -Brooks Cole* (2011).
20. Arkles, B. Hydrophobicity, hydrophilicity and silanes. *Paint and Coatings Industry* **22**, 114–135 (2006).
21. Jenkins A. J. Surface Design: Applications in Bioscience and Nanotechnology P. 471. ISBN 978-3-527-40789-7. (2009)
22. Young T. An essay on the cohesion of fluids. *Phil. Trans. R. Soc*. 9565–87 (1805)

23. Gibbs, J.W. On the Equilibrium of Heterogeneous Substances. The Scientific Papers of J. Willard Gibbs pp. 55–354, ISBN 978-0918024770 (1876-1878)
24. Luo, S. *et al.* Stability and rheology of three types of W/O/W multiple emulsions emulsified with lecithin. *J Dispers Sci Technol* **38**, 1530–1535 (2017).
25. Zhi, Z., Liu, R., Wang, W., Dewettinck, K. & Van Bockstaele, F. Recent progress in oil-in-water-in-oil (O/W/O) double emulsions. *Crit Rev Food Sci Nutr* **0**, 1–12 (2022).
26. Everett, D. H. & Butterworths, L. International union of pure and applied chemistry division of physical chemistry. Manual of symbols and terminology for physicochemical quantities and units . Appendix II: Definitions, Terminology and Symbols in Colloid and Surface Chemistry PART I. 579–638 (1972).
27. Tcholakova, S., Denkov, N. D. & Lipsb, A. Comparison of solid particles, globular proteins and surfactants as emulsifier. *Phys. Chem. Chem. Phys.* **10**, 1608–1627 (2008).Chevalier, Y. & Bolzinger, M. A. Emulsions stabilized with solid nanoparticles: Pickering emulsions. *Colloids Surf A Physicochem Eng Asp* **439**, 23–34 (2013).
28. Robert Aveyard , Bernard P. Binks*, J. H. C. Emulsions stabilised solely by colloidal particles. *Adv. Colloid Interface Sci.* **5766 LNCS**, 503–546 (2002).
29. Binks, B. P., Rodrigues, J. A. & Frith, W. J. Synergistic interaction in emulsions stabilized by a mixture of silica nanoparticles and cationic surfactant. *Langmuir* **23**, 3626–3636 (2007).
30. Haase, M. F. Modification of Nanoparticle-Surfaces for Emulsion Stabilization and Encapsulation of Active Molecules for Anti-Corrosive Coatings. *Phd thesis* (2011).
31. Ikem, V. O., Menner, A., Bismarck, A. & Norman, L. R. Particles as surfactants: similarities and differences. *SPE J.* **19**, 437–442 (2014).
32. Mohraz, A. Emulsions: Simple shaking yields bicontinuity. *Nat. Nanotechnol.* **12**, 1021–1022 (2017).K. Stratford, R. Adhikari, I. Pagonabarraga, J.-C. Desplat & M. E. Cates. Colloidal Jamming at Interfaces: A Route to Fluid-Bicontinuous Gels. *Science (1979)* **309**, 2195–2198 (2005).
33. Herzig, E. M., White, K. A., Schofield, A. B., Poon, W. C. K. & Clegg, P. S. Bicontinuous emulsions stabilized solely by colloidal particles. *Nat Mater* **6**, 966–971 (2007).
34. Haase, M. F. *et al.* Multifunctional nanocomposite hollow fiber membranes by solvent transfer induced phase separation. *Nat Commun* **8**, (2017).
35. Khan, M. A. *et al.* Nanostructured, Fluid-Bicontinuous Gels for Continuous-Flow Liquid–Liquid Extraction. *Advanced Materials* **34**, (2022).
36. Cahn, J. W. On Spinodal Decomposition. *Acta Metallurgica, volume 9, Issue 9 (1961)*
37. Binks, B. P., Duncumb, B. & Murakami, R. Effect of pH and salt concentration on the phase inversion of particle-stabilized foams. *Langmuir* **23**, 9143–9146 (2007).
38. Prinsen, M. J. Resolving Oil-to-Water Channel Leakage in Bijels, Master Thesis (2022).